Journal Pre-proof

Altered Microbiota by a High-Fat Diet Accelerates Lethal Myeloid Hematopoiesis Associated with Systemic Socs3 Deficiency

Kaori Cho, Takashi Ushiki, Hajime Ishiguro, Suguru Tamura, Masaya Araki, Tatsuya Suwabe, Takayuki Katagiri, Mari Watanabe, Yoko Fujimoto, Riuko Ohashi, Yoichi Ajioka, Ippei Shimizu, Shujiro Okuda, Masayoshi Masuko, Yoshimi Nakagawa, Hideyo Hirai, Warren S. Alexander, Hitoshi Shimano, Hirohito Sone

PII: S2589-0042(21)01085-3

DOI: https://doi.org/10.1016/j.isci.2021.103117

Reference: ISCI 103117

To appear in: *ISCIENCE*

Received Date: 20 August 2020

Revised Date: 10 August 2021

Accepted Date: 9 September 2021

Please cite this article as: Cho, K., Ushiki, T., Ishiguro, H., Tamura, S., Araki, M., Suwabe, T., Katagiri, T., Watanabe, M., Fujimoto, Y., Ohashi, R., Ajioka, Y., Shimizu, I., Okuda, S., Masuko, M., Nakagawa, Y., Hirai, H., Alexander, W.S., Shimano, H., Sone, H., Altered Microbiota by a High-Fat Diet Accelerates Lethal Myeloid Hematopoiesis Associated with Systemic Socs3 Deficiency, *ISCIENCE* (2021), doi: https://doi.org/10.1016/j.isci.2021.103117.

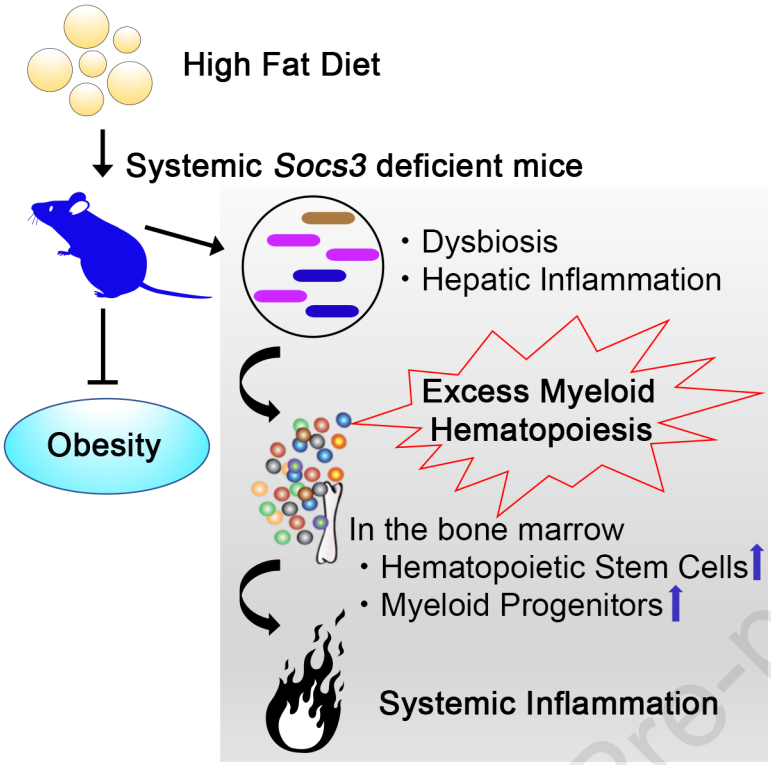

Altered Microbiota by a High-Fat Diet Accelerates Lethal Myeloid Hematopoiesis Associated with Systemic Socs3 Deficiency

Kaori Cho[1,13], Takashi Ushiki[1,2,14,★], Hajime Ishiguro[1,13], Suguru Tamura[1], Masaya Araki[3], Tatsuya Suwabe[1], Takayuki Katagiri[1], Mari Watanabe[2], Yoko Fujimoto[2], Riuko Ohashi[4,5], Yoichi Ajioka[4,5], Ippei Shimizu[6], Shujiro Okuda[7], Masayoshi Masuko[1], Yoshimi Nakagawa[8], Hideyo Hirai[9,10], Warren S. Alexander[11,12], Hitoshi Shimano[3] and Hirohito Sone[1]

1) Department of Hematology, Endocrinology and Metabolism, Faculty of Medicine, Niigata University, Niigata City, Niigata 951-8510, Japan

2) Department of Transfusion Medicine, Cell Therapy and Regenerative Medicine, Niigata University Medical and Dental Hospital, Niigata City, Niigata 951-8520, Japan

3) Department of Endocrinology and Metabolism, Faculty of Medicine, University of Tsukuba, Tsukuba City, Ibaraki 305-8575, Japan

4) Histopathology Core Facility, Faculty of Medicine, Niigata University, Niigata City, Niigata 951-8510, Japan

5) Division of Molecular and Diagnostic Pathology, Niigata University Graduate School of Medical and Dental Sciences, Niigata City, Niigata 951-8510, Japan

6) Department of Cardiovascular Biology and Medicine, Juntendo University Graduate School of Medicine, Bunkyo-ku, Tokyo 113-8421, Japan

7) Division of Bioinformatics, Niigata University Graduate School of Medical and Dental Sciences, Niigata City, Niigata 951-8510, Japan

8) Division of Complex Biosystem Research, Department of Research and Development, Institute of Natural Medicine, University of Toyama, Toyama City, Toyama 930-0194, Japan

9) Department of Clinical Laboratory Medicine, Kyoto University Hospital, Kyoto City, Kyoto 606-8507, Japan

10) Laboratory of Stem Cell Regulation, School of Life Sciences, Tokyo University of

Pharmacy and Life Sciences, Hachioji City, Tokyo 192-0392, Japan

11) Blood Cells and Blood Cancer Division, The Walter and Eliza Hall Institute of Medical Research, Parkville, Victoria 3052, Australia

12) Department of Medical Biology, The University of Melbourne, Parkville, Victoria 3052, Australia

13) These authors contributed equally

14) Lead Contact

★ Correspondence

Correspondence to

Takashi Ushiki, MD, PhD,

Department of Transfusion Medicine, Cell Therapy and Regenerative Medicine, Niigata University Medical and Dental Hospital

1-754 Asahimachi-dori, Chuo-ku, Niigata City, Niigata 951-8520, Japan

E-mail: tushiki@med.niigata-u.ac.jp

SUMMARY

The Suppressors of Cytokine Signaling (SOCS) proteins are negative regulators of cytokine signaling required to prevent excessive cellular responses. In particular, SOCS3 is involved in the regulation of metabolic syndromes, such as obesity and diabetes, by suppressing leptin and insulin signals. SOCS3 also suppresses the inflammatory response associated with metabolic stress, but this specific role remains undefined. Wild-type mice on a high-fat diet (HFD) exhibited only fatty liver, whereas systemic deletion of SOCS3 resulted in excessive myeloid hematopoiesis and hepatic inflammation. In addition, depletion of the gut microbiota resulted in considerable improvement in excess granulopoiesis and splenomegaly, halting the progression of systemic inflammation in SOCS3KO mice on the HFD. This result suggests that intestinal dysbiosis is involved in inflammation associated with SOCS3KO. Although contributing to diet-induced obesity and fatty liver, SOCS3 is nevertheless critical to suppress excess myeloid hematopoiesis and severe systemic inflammation associated with intestinal dysbiosis on HFD.

INTRODUCTION

High fat diets (HFDs) accelerate chronic diseases such as type 2 diabetes mellitus, cardiovascular disease, inflammatory bowel disease, allergy, and certain types of cancer via low grade inflammation. The inflammatory environment develops in the central nervous system, including the hypothalamus, and in the peripheral tissues, including the liver, adipose tissue, skeletal muscle, and intestine (Duan et al., 2018). In recent years, it has been revealed that HFD affects bone marrow components and hematopoietic stem cell (HSC) homeostasis through gut bacteria dysbiosis. For example, HFD loading alters the gut microbiota and changes the bone marrow niche by increasing ectopic fat accumulation in bone marrow, increasing fatty marrow via the activation of peroxisome proliferator-activated receptor γ2 (PPARγ2) and shifts hematopoietic stem cells toward granulocyte hematopoiesis (Luo et al., 2015). In addition, in *Spred1* knockout mice, abnormalities in the intestinal flora contribute to enhanced ERK signaling in HSCs, causing marked granulocyte hyperplasia, and this phenomenon is alleviated by depletion of the gut microbiota (Tadokoro et al., 2018). These dysbiosis-mediated abnormalities in the gut may be important for controlling low-grade inflammation via hematopoiesis, but

79 the detailed mechanisms and regulators of the intestinal-blood cell association remain
80 unclear.

81 The SOCS family is required to prevent spontaneous inflammation associated with
82 excessive cytokine responses. The SOCS family contains eight proteins, SOCS1-7 and
83 CIS (cytokine inducible SH2 containing protein), and is characterized by the presence of
84 an SH2 domain that mediates interaction with signaling proteins, such as the JAK kinases
85 and/or cytokine receptors, and a C-terminal SOCS Box motif. Regulation of signaling by
86 IL-6 and G-CSF by SOCS3 appears to be important in preventing inflammation (Croker
87 et al., 2003; Croker et al., 2004). Furthermore, SOCS3 is strongly associated with obesity
88 and insulin resistance. Inhibition of SOCS3 in obese mice improves insulin sensitivity
89 and fatty liver, and it also normalizes the increased expression of sterol regulatory element
90 binding protein (SREBP)-1c, which is the key regulator of fatty acid synthesis in the liver
91 (Ueki et al., 2004). These findings indicate that the inhibition of SOCS3 is a promising
92 therapeutic target for improving glucose tolerance and HFD-induced inflammatory
93 effects.

Herein, we show systemic homozygous SOCS3 knockout (KO) results in marked myeloid hematopoiesis and lethal inflammation under conditions of HFD loading. In these mice, myeloid cells invaded the liver and eventually caused systemic inflammation; however, inflammation was substantially improved by depletion of the gut microbiota using antibiotics.

RESULTS

Generation of mice lacking SOCS3 on the HFD diet

Complete SOCS3 deficiency in mice causes embryonic lethality due to the uncontrolled actions of leukemia inhibitory factor signaling (Roberts et al., 2001). To overcome the embryonic lethality of SOCS3 deficiency, we used a tamoxifen-inducible Cre-recombinase, *Rosa26-CreERT2* in combination with a homozygous floxed SOCS3 allele (*Socs3*$^{fl/fl}$). To investigate the significant roles of SOCS3 in HFD, *Socs3*-knockout (KO) genotypes were generated by treatment with tamoxifen. To explore the combined effect of both SOCS3 deficiency and HFD-load in inflammation, mice were established as indicated: SOCS3 deficiency in mice on HFD diet (*S3-HFD*, tamoxifen-treated *Socs3*$^{fl/fl}$*; Rosa26-CreERT2*) or control chow (*S3-chow*, tamoxifen-treated *Socs3*$^{fl/fl}$*; Rosa26-*

111 *CreERT2*); functionally normal SOCS3 on HFD diet (*WT-HFD*, vehicle-treated *Socs3*$^{fl/fl}$*;*
112 *Rosa26-CreERT2*) or on control chow (*WT-chow*, vehicle-treated *Socs3*$^{fl/fl}$*; Rosa26-*
113 *CreERT2*) (Fig S1). Previously, we confirmed highly efficient Cre-ERT2-dependent
114 recombination of the floxed *Socs3* allele in the hematopoietic organs of tamoxifen-, but
115 not vehicle-treated mice, using Southern blotting (Ushiki et al., 2016). Near-complete
116 tamoxifen-induced inactivation of the *Socs3* allele was also confirmed in the trunk of
117 *Socs3* deficient mice, but not in intracranial organs, using genomic PCR (Fig S2).

118 **SOCS3KO protected against diet-induced obesity and fatty liver, and improved**
119 **blood glucose concentration without increasing activity and energy metabolism**

120 The S3-chow mice were lighter than WT-chow mice at 28 weeks of age. Furthermore,
121 mice fed the HFD (WT-HFD) developed obesity; however, S3-HFD mice were
122 significantly protected from diet-induced obesity. Thus, SOCS3KO restricts weight gain,
123 especially that caused by HFD (Fig 1A). As for food intake at 15 weeks of age, intake
124 (g/day) did not differ with HFD. Caloric intake (kcal/day) in WT-HFD was significantly
125 higher than that in WT-chow, and the same was observed in S3-HFD compared with that
126 in S3-chow. However, the intake (kcal/day) in WT-HFD and S3-HFD did not differ

127 significantly (Fig 1B). Lipid intake (g/day) displayed the same trend as caloric intake. A
128 significant increase between chow and HFD was evident in both WT and SOCS3-
129 deficient models (Fig 1C). Therefore, the amount of food and the nutritional value of the
130 food ingested cannot explain the significant weight difference observed between WT and
131 SOCS3-deficient mice on the HFD. In parallel with the body weight change, the
132 development of fatty liver and secretion of liver triglyceride (TG) were suppressed in S3-
133 HFD mice on day 30 after tamoxifen treatment (Fig 1D, E) and myeloid infiltrations were
134 observed in SOCS3-deficient mice (Fig 1D). Regarding movement, on day 30 after
135 tamoxifen treatment, open field total distance was lower in the HFD group than in the
136 control diet group in WT mice. The total distance was low in the chow group, and it did
137 not change with HFD feeding in SOCS3-deficient mice (Fig 1F). The open field total
138 movement duration agreed with the total distance trend observed (Fig 1G). The rotary
139 momentum test revealed lower scores in WT-HFD mice than in normal diet. The scores
140 of both SOCS3-deficient groups, HFD and normal diet, were lower than those of WT-
141 chow mice on day 30 after tamoxifen treatment (Fig 1H). Respiratory exchange ratio
142 appeared low in the HFD groups, for both WT and SOCS3-deficient mice, on day 30 after

143 tamoxifen (Fig 1I). Blood glucose levels were higher in the WT-HFD group than in the
144 S3-chow group, but there was no other difference (Fig 1J). Insulin resistance testing
145 indicated lower blood glucose level in SOCS3KO mice than in WT mice on day 14 after
146 tamoxifen treatment (Fig 1K), suggesting that the systemic effects of SOCS3-deficiency
147 improved HFD-induced insulin resistance.
148 It has been reported that the circulating leptin concentration is higher in wild-type mice
149 on an HFD than in mice on chow, whereas the leptin concentration in SOCS3
150 haploinsufficient mice on an HFD is not significantly higher than that in mice on chow
151 (Howard et al., 2004). Consistent with this, the plasma leptin level was significantly
152 increased by HFD in WT mice, and this was alleviated in S3 mice (Fig 1L).
153 Thus, SOCS3 deficiency ameliorated HFD-induced obesity and hepatic lipid secretion
154 that cannot be attributed to improved metabolism and increased energy expenditure alone.
155 In some cases, various types of tumors develop or are promoted in SOCS3-deficient mice
156 including gastric and pancreatic cancer (Inagaki-Ohara et al., 2014; Lesina et al., 2011).
157 These neoplasms were not detected on day 30 after tamoxifen in all phenotypes examined
158 (Table S1). Thus, neoplasm is not associated with obesity resistance.

SOCS3 deficiency combined with HFD induces rapid inflammatory disease with myeloid hematopoiesis

While SOCS3-deficiency improved obesity and fatty liver, the mice rapidly became unwell when fed the HFD from day 32 after tamoxifen treatment, and their median survival was 65.5 days after tamoxifen-induced deletion of SOCS3. In contrast, several S3-chow mice became moribund from day 106 after tamoxifen treatment; however, they did not reach 50% mean survival over a 6-month observation period. The control group mice (WT-chow, WT-HFD) did not become unwell (Fig 2A). All mice were analyzed upon initial signs of disease (hereinafter referred to as moribund). Inflammation was observed in the spleen and liver from day 30 after tamoxifen administration; thus, we defined this period as the pre-inflammation phase. Only S3-HFD mice showed marked neutrophilia in the blood (Fig 2B) and considerable splenomegaly (Fig 2C) in the pre-inflammation phase. Furthermore, S3-chow mice subsequently exhibited splenomegaly around the median survival time. Thus, SOCS3KO mice on a normal diet developed splenomegaly; however, spleen weight of these mice was significantly lower than that of the S3-HFD group and neutrophilia was not observed (Fig 2D, E). Thus, HFD is

necessary to induce neutrophilia and more significant splenomegaly. Pathological analysis revealed that the S3-HFD group displayed hepatic inflammation without fatty liver in the pre-inflammation phase. Moribund S3-HFD mice often displayed inflammatory skin lesions such as pachyderma, alopecia, and/or ulcers (Fig 2F), and autopsies also revealed splenomegaly, lymphadenopathy, and inflammation in the liver, fat, lung, and kidney (Fig 2G). Thus, as SOCS3-deficient mice on normal chow or WT mice on the HFD did not display excessive granulopoiesis, the combination of SOCS3 deficiency and HFD induced rapid granulopoiesis from day 30 after tamoxifen treatment, suggesting that granulopoiesis contributed to systemic inflammation.

SOCS3 deficiency induced granulopoiesis in the spleen

Lymphoid follicle structure collapsed due to increasing numbers of $CD11b^{+}Gr\text{-}1^{+}$ granulocytes in the spleen (Fig 3A, B) under SOCS3 deficiency, but the percentage of granulocytes was significantly higher in the S3-HFD group than in the S3-chow group. Next, we investigated granulocyte maturation in the spleen in the pre-inflammation phase (Fig 3C). In brief, hematopoietic cells undergoing granulopoiesis were separated into subpopulations #1 to #5 by FACS analysis using c-Kit and Ly-6G markers, and

granulocyte differentiation and maturation stages were classified as follows: Subpopulation #1 comprised mainly myeloblasts, #2 contained an abundance of promyelocytes, #3 mainly myelocytes, #4 mainly metamyelocytes, and #5 mainly band cells and segmented cells. Cells undergoing granulocytic maturation (#4-#5) were predominant in SOCS3KO mice on both normal chow and HFD (Fig 3D). In addition, considering the extensive splenomegaly in S3-HFD, mature granulopoiesis is likely more active in the S3-HFD group than the S3-chow group. Colony assays revealed increased myeloid progenitor cells (CFU-GM, CFU-G, and CFU-M) in the spleen in SOCS3-deficient mice, with the HFD driving higher numbers of myeloid progenitor colonies in S3-HFD mice (Fig 3E). Thus, SOCS3 deficiency enhanced granulopoiesis without HFD in the spleen and maturation of granulocytes was similar in the S3-chow and S3-HFD groups. However, hematopoiesis indicated by myeloid progenitor cell number was significantly higher in the S3-HFD group than in the S3-chow group.

SOCS3 deficiency with HFD feeding accelerates hepatic inflammation without obesity and ectopic fat accumulation

206 SOCS3 deficiency improved HFD-induced obesity and ectopic fat accumulation (Fig 1A,
207 E); however, myeloid infiltration was observed in the liver. These myeloid cells were
208 observed in the entire liver, including the hepatic vein area, portal region, and liver
209 parenchyma on day 30 after tamoxifen treatment during the pre-inflammation phase (Fig
210 4A). Additionally, analysis was performed on day 14 post-tamoxifen treatment, but at
211 this time hepatic infiltration and splenomegaly were not observed, and in the serum, liver
212 enzyme activities did not differ among the groups. The total cholesterol level was higher
213 in the S3-HFD and WT-HFD groups than in the S3-chow and WT-chow groups (Fig 4B).
214 In the pre-inflammatory phase (day 30 after tamoxifen treatment), the inflammation
215 marker TNF-α was increased in the liver, but IL-6 in the S3-HFD group did not mirror
216 this trend. Unexpectedly, marked Ly6G RNA expression was observed in the S3-HFD
217 group, indicating excess neutrophil infiltration and blood cells in the liver as local
218 inflammation (Fig 4C). Furthermore, elevation in CD11b, CD14, and CD68 RNA
219 expression indicated monocyte and macrophage infiltration in the liver in the S3-HFD
220 group. Although inflammasome markers IL-1β and Caspase-1 were not increased in the
221 pre-inflammation phase (Fig 4D) in all phenotypes (day 30 after tamoxifen treatment),

these genes were significantly increased in the S3-HFD group in the moribund phase (day 65 post-tamoxifen treatment) (Fig 4E).

Furthermore, fatty acid synthetase including, fatty acid desaturase 1 (FADS-1), stearoyl-CoA desaturase 1 (SCD-1), elongation of very long chain fatty acids 6 (Elovl6), and Sterol regulatory element binding protein 1 (SREBP-1) were present in the pre-inflammation phase (Oishi et al., 2017). The results indicated that FADS-1 was elevated by the HFD in the WT-HFD group, but this increase was abolished in the absence of SOCS3. In addition, *SCD-1* expression was lower in the WT-HFD group than in the WT-chow group, and *SCD-1* expression was low in the SOCS3-deficient groups, irrespective of diet. As fatty acid synthetase *FADS-1* is classified as an anti-inflammatory gene (Gromovsky et al., 2018) and *SCD-1* is classified as an inflammatory gene (Liu et al., 2010), intra-hepatic environment cannot be predicted only by fatty acid synthetase in the S3-HFD group. Regarding fat synthesis, low expression of *FADS-1* and *SCD-1* suppressed fat synthesis in the liver. SREBP-1 and Elovl6 expression levels were unchanged across all phenotypes (Fig S3).

Hematopoietic SOCS3KO is not involved in HFD-induced inflammation and is not a direct pro-inflammatory factor

Given the excessive granulocyte infiltration into the liver, we next considered the specific role of hematopoietic loss of SOCS3. Mature myeloid-specific SOCS3KO mice (*LysM*; *LysMCre Socs3*$^{fl/fl}$) were fed the HFD from 4 weeks of age. In *LysMCre Socs3*$^{fl/fl}$ mice, SOCS3 was partially deleted in peripheral white blood cells and intraperitoneal cells (Fig S4). While systemic lethal inflammation was not observed, HFD-induced obesity was present in mature myeloid-specific SOCS3KO mice on the HFD (Fig 5A, B). Myeloid-specific SOCS3KO mice exhibited mild HFD-induced fatty liver (Fig 5C); however SOCS3 deficiency showed there were trends of decrease in liver lipids in contrast to those in WT, thereby suppressing fatty liver in myeloid-specific SOCS3KO mice (Fig 5D). Inflammation was not observed in myeloid-specific SOCS3KO mice (Fig 5C). In addition, granulocytosis in peripheral blood and splenomegaly were not observed (Fig 5E, F). Next, we investigated the effect of deletion of SOCS3 in the entire hematopoietic system, including myeloid progenitors, using Vav-cre (*VavCre Socs3*$^{fl/fl}$). In *VavCre Socs3*$^{fl/fl}$ mice, SOCS3 was completely deleted in peripheral white blood cells (Fig S4). The results

253 in *VavCre Socs3*$^{fl/fl}$ mice were similar to those in *LysMCre Socs3*$^{fl/fl}$ mice: hepatic
254 inflammation and excess neutrophilia-related systemic inflammation were not observed
255 (Fig 5G, I). Hematopoietic-specific SOCS3KO mice displayed mild fatty liver (Fig 5G,
256 H), but granulocytosis was not evident (Fig 5I, J). Differentiation and maturation of
257 neutrophils in the spleen did not significantly differ between the *VavCre Socs3*$^{fl/fl}$ mice
258 and controls (Fig 5K). These data suggest that the loss of SOCS3 in blood cells is not
259 likely to be the cause of systemic inflammation, rather non-hematopoietic SOCS3 appears
260 to be important.

261 **Intestinal tract is the source of HFD-induced inflammation and depletion of the gut**
262 **microbiota abolishes inflammation**

263 Considering the above results, and given the link among diet, gut biota, and hematopoiesis
264 as previously described (Luo et al., 2015; Tadokoro et al., 2018), a meta 16S rRNA gene
265 sequencing analysis of intestinal microbiota was performed. The principal coordinate
266 analysis showed genetic differences among microbiota in all groups of mice (Fig 6A).
267 Phylogenetic classification showed reduced *Bifidobacteriales* members in the HFD
268 groups, including S3-HFD and WT-HFD. These were significantly altered by depletion

of the gut microbiota with a cocktail of four antibiotics (4Abx, see Materials and Methods) and phylogenetic classification indicated a dominance in *Lactobacillales* abundance in not only the HFD groups, but also the chow groups (Fig 6B). The survival of the S3-HFD group significantly improved following 4Abx treatment (Fig 6C). Thus, the intestinal tract was demonstrated as the primary inflammation-initiating organ. Interestingly, both granulopoiesis and splenomegaly were substantially reduced in the S3-HFD group (Fig 6D-F), whereas there were no effects of 4Abx treatment on survival or granulopoiesis in WT mice. In addition, altered granulocyte-maturation in the spleen was also significantly reduced by microbiota depletion in S3-HFD mice (Fig 6G). mRNA levels of *TNF-α* in the colon decreased across all phenotypes after microbiota depletion (Fig 6H). Therefore, depletion of the gut microbiota might also suppress colon inflammation by improving dysbiosis. The data suggest that SOCS3 plays a key role in controlling systemic inflammation caused by enteric bacteria in the context of an HFD.

Intestinal tract microbiota depletion improves myeloid hematopoiesis in S3-HFD mice

Next, we checked the serum cytokine/chemokine levels that could affect granulopoiesis and inflammation. Although the differences were not statistically significant, GM-CSF, IL-17A, CCL-2, and CCL-4 were higher in S3-HFD mice than in WT mice, and normalized by the depletion of the gut microbiota. IL-6 and S100A8/A9 were higher in S3-chow than in WT, however compositions of gut microbiota such as *Bifidobacteriales* and *Clostridiales* are similar in S3-chow and WT-HFD, indicating SOCS3 deficiency itself potentially contributed to elevation of these cytokines. In addition, levels of these cytokines were reduced by the depletion of gut microbiota, indicating these cytokines were enhanced by gut microbiota-associated inflammation. Although, gene expression of TNF-α in the liver of S3-HFD mice was high (Fig 4), there were no differences in the serum protein levels (Fig 7A). Regarding the origin of IL-17A from Th17 cells, which are abundant in the gut, especially the duodenum (Esplugues et al., 2011), we checked IL-17A- and IL-17-related genes in the duodenum. In addition, Th17 cells also express the chemokine receptor CCR6 in a cell-specific manner. However, there was no significant difference in the expression levels of IL-17A- and IL-17-related genes and CCR6 between WT and SOCS3-deficient mice in the duodenum before microbiota

depletion (Fig S5). Regarding hematopoiesis in the bone marrow (BM), myeloid hyperplasia persisted in SOCS3-deficient mice with microbiota depletion (Table S1), and Gram staining revealed no bacteria in all groups (Table S2). In addition, hematopoietic stem cells (Lineage^{-}Sca-1^{+}c-Kit^{+}; LSK cells and CD34^{-} LSK cells) and myeloid progenitors (common myeloid progenitor; CMP and granulocyte-macrophage progenitor; GMP) were significantly higher in S3-HFD mice than WT mice. However, these differences were variably alleviated by 4Abx treatment (Fig 7B). Combined with the observation that the elevated leukocyte count observed in S3-HFD mice was reversed by microbiota depletion, the existence of myeloproliferative diseases was unlikely in these mice.

DISCUSSION

Previously, systemic SOCS3 haploinsufficiency has been shown to attenuate diet-induced obesity by improving insulin resistance and enhancing leptin sensitivity (Howard et al., 2004). Thus, SOCS3KO is expected to improve obesity and obesity-associated metabolic complications. In fact, while aortic dissection is associated with arteriosclerosis

316 or hypertension, smooth muscle specific SOCS3KO (Hirakata et al., 2020) or conversely
317 SOCS3 expression in macrophages (Ohno-Urabe et al., 2018) protected against aortic
318 dissection via inflammation control. However, systemic homogenous SOCS3KO resulted
319 in systemic inflammation due to excess myeloid hematopoiesis, particularly
320 granulopoiesis. SOCS3 is reportedly associated with HFD-induced low-grade
321 inflammation in local organs (Duan et al., 2018; Sachithanandan et al., 2010), however,
322 obvious systemic inflammation and excess granulopoiesis has not been reported.
323 Systemic haploinsufficiency or neural cell-specific SOCS3KO was originally reported
324 to enhance hypothalamic leptin signals and reduce weight gain in mice on an HFD
325 (Howard et al., 2004; Mori et al., 2004). In our study, mice were fed an HFD to examine
326 "systemic" homogenous SOCS3KO effects on obesity. The results demonstrated that
327 there were no differences in dietary intake across all genotypes, thus the amounts of
328 consumed calories and fat intake were the same between the S3-HFD and WT-HFD
329 groups. As tamoxifen cannot easily transit the blood–brain barrier, Cre recombinase
330 cannot be efficiently released in the CreERT system in intracranial organs. In turn, this
331 resulted in low SOCS3 deletion rates and presumably no accentuation of leptin signals in

intracranial organs, including the hypothalamus. SOCS3KO mice on the HFD received high calories without increasing activity and energy consumption. In addition, the phenotype differed from brain-specific SOCS3KO mice (Mori et al., 2004), especially regarding appetite. Systemic inflammation was suspected to be strongly associated with obesity resistance in systemic SOCS3KO, rather than enhanced leptin signaling. In fact, the serum leptin level was not increased in SOCS3KO mice on the HFD.

Similar phenomena have been observed in organ-specific SOCS3KO mice. Liver-specific SOCS3KO mice exhibited improved insulin resistance on the control diet; however, liver-specific KO mice on the HFD exhibited increased hypothalamic SOCS3 expression and fatty acid synthase expression. Finally, liver-specific KO mice on the HFD displayed obesity and hepatic inflammation (Sachithanandan et al., 2010). In this study, hepatic inflammation was observed with an increase in F4/80-positive cells, and hepatic gene expression and plasma levels of TNF-α and IL-6 were also elevated, indicating that independent hepatic SOCS3KO can potentially induce low-grade inflammation. In our study, systemic SOCS3KO also showed low-grade inflammation similar to hepatic SOCS3KO; however, this inflammation was attenuated by the depletion of the gut

348 microbiota. These phenomena indicated gut dysbiosis accelerated hepatic inflammation.
349 Skeletal muscle-specific SOCS3KO mice displayed improved insulin resistance
350 (Jorgensen et al., 2013). It has been confirmed that skeletal muscle damage in SOCS3KO
351 mature muscle fibers did not improve muscle regeneration, but tended to induce an
352 inflammatory response with elevated TNF-α and macrophage infiltration in muscles
353 (Swiderski et al., 2016).
354 As for fatty liver, here, systemic SOCS3 deficiency clearly improved fatty liver
355 compared to that in wild-type mice on the HFD. The phosphorylation of STAT signal
356 transducers is important against both inflammation and metabolism. For example, the
357 level of IL-6 and phosphorylation of STAT3 signaling in hepatocytes are reported to
358 change hepatic metabolism toward the suppression of hepatic glucose production (Inoue
359 et al., 2006), or to improve fatty liver on a choline-deficient, ethionine-supplemented diet
360 (Kroy et al., 2010). In our model, hepatic *IL-6* gene expression was not different, but
361 serum IL-6 level was significantly elevated in SOCS3-deficient mice compared with that
362 in wild-type mice in the Luminex assay. In addition, SOCS3 deficiency can result in
363 prolonged phosphorylation of STAT3 signaling (Ushiki et al., 2016); thus, a high serum

IL-6 level with SOCS3 deficiency might be one of the factors that contribute to improving fatty liver.

We previously demonstrated a rapid inflammation and neutrophilia in mice lacking both SOCS1 and SOCS3 in hematopoietic cells (Ushiki et al., 2016). We showed that SOCS1KO and SOCS3KO independently modulate the proliferation and activation of lymphoid and myeloid cells in the onset of rapid inflammatory disease. In brief, excessive $CD8^+$ $CD44^{hi}$ T cells, a defining feature of the absence of SOCS1 (Cornish et al., 2003; Davey et al., 2005), were observed and increased auto-reactive $CD8^+$ T cells underpins the autoimmunity in SOCS1-deficient mice (Davey et al., 2005). Our previous data were extended to this model to suggest that the absence of SOCS3, in the already pro-inflammatory environment established by SOCS1 deficiency, results in hyper-responsiveness of immune cells to cytokines, such as G-CSF and IL-6, even in modest amounts, and substantially accelerates myeloid proliferation and inflammatory infiltration of the target tissues (Ushiki et al., 2016). Thus, a lack of SOCS3 alone in hematopoietic cells did not result in disease development (Croker et al., 2012); however, SOCS3KO could accelerate inflammation via excessive granulopoiesis (Ushiki et al.,

2016). Thus, regarding granulopoiesis in the current study, stimulation from activated T cell or low-grade inflammation by metabolic stress may be involved in granulocyte proliferation in SOCS3KO hematopoiesis. Our results suggest that GM-CSF, IL-17A, CCL-2, and CCL-4 are candidates as cytokines/chemokines that may contribute to systemic inflammation in S3-HFD mice and worthy of further study. As for IL-17A, SOCS3 is known to suppress Th17 differentiation (Chen et al., 2006; Qin et al., 2009), and Th17 cells are also known to be abundant in the gut (Esplugues et al., 2011). In our study, IL-17A and related gene expression in the duodenum of S3-HFD did not differ from those in other groups. Thus, IL-17 may be secreted from other organs that show local inflammation.

The effects of an HFD on hematopoiesis are also becoming apparent. HFD decreases the number of long-term LSK cells and shifts hematopoiesis from lymphoid to myeloid differentiation at the progenitor cell level (Luo et al., 2015). HFD also affects the bone marrow by altering the gut microbiota (Luo et al., 2015). In our experiments, myeloid cell-infiltration was observed in the spleen and liver in the S3-HFD group. However, this inflammation was not seen in myeloid-specific SOCS3KO mice. This indicates that

396 excess myeloid hematopoiesis in the S3-HFD group requires the involvement of intestinal
397 and hepatic inflammation, rather than the direct effects of HFD or SOCS3 deficiency on
398 blood cells. In fact, LSK and myeloid progenitors indicated shifts to myeloid
399 differentiation from the hematopoietic stem cell-level in S3-HFD mice in our study. BM
400 histopathology also showed myeloid hyperplasia, slight erythroid hypoplasia, and
401 megakaryocytosis features resembling chronic myeloid leukemia feature. However,
402 myeloid hematopoiesis was significantly reduced in the BM and peripheral blood in
403 response to depletion of the gut microbiota, indicating that myeloid proliferation was
404 reversible and likely to have a crucial role in the systemic inflammation development in
405 S3-deficient mice on the HFD.

406 Suppression of the gut microbiota substantially alleviated myeloid hematopoiesis and
407 halted the progression of systemic inflammation in S3-HFD mice. In addition, the gut
408 microbiota composition was altered by antibiotic treatment to primarily enrich
409 *Lactobacillales* in all groups. It has been reported that HFD chronically increased plasma
410 bacterial lipopolysaccharide (LPS) levels by increasing the proportion of LPS-containing
411 microbiota in the gut, called metabolic endotoxemia. In our study, *Bifidobacteriales*

412 members were reduced in the HFD groups (Turnbaugh et al., 2006). Bifidobacteria are
413 known to reduce intestinal LPS levels and improve mucosal barrier function (Cani et al.,
414 2007b). Thus, the HFD groups are suspected to be sensitive to HFD-induced low-grade
415 inflammation. Furthermore, various myeloid cells, such as granulocytes, monocytes, and
416 macrophages, infiltrated the liver due to HFD-induced metabolic stress in our study. LPS
417 receptor CD14-mutant mice on an HFD did not exhibit inflammation in the adipose tissue
418 and liver, whereas insulin sensitivity was improved (Cani et al., 2007a). This suggests
419 that CD14 cells in S3-HFD mice might enhance metabolic endotoxemia. It has also been
420 shown that bacteria belonging to *Clostridiales* can induce Treg differentiation (Atarashi
421 et al., 2011; Furusawa et al., 2013). We showed that SOCS3KO mice on an HFD
422 displayed a slight decrease in *Clostridiales* in contrast to WT mice on an HFD. Thus,
423 dysbiosis could affect the pro-inflammatory environment in SOCS3KO mice on an HFD.
424 In conclusion, SOCS3 is strongly associated with excess myeloid hematopoiesis in the
425 context of the HFD. SOCS3 deficiency may cause resistance to diet-induced obesity, but
426 also causes severe systemic inflammation accompanying HFD-induced microbiota

427 alteration. Therefore, although SOCS3 could be a therapeutic target for obesity, potent
428 inflammatory adverse reaction should be taken into account.

429

430 **Limitations of the study**

431 This study shows that systemic deletion of SOCS3 results in excessive myeloid
432 hematopoiesis and hepatic inflammation, which are dependent on gut microbiota.
433 Moreover, SOCS3 crucially regulates intestinal dysbiosis-mediated inflammation with
434 high fat diet. However, it is currently unclear how a high-fat diet can alter the composition
435 of the gut microbiota. Similarly, future studies will further define the specific roles of
436 SOCS3 in regulation of the gut microbiota and systemic inflammation in this context.

437

438 **ACKNOWLEDGMENTS**

439 The authors acknowledge Ms. Junko Kumagai and Mr. Kenji Oyachi (Histopathology
440 Core Facility, Faculty of Medicine, Niigata University, Niigata, Japan) for special
441 technical support in pathological analysis. This study was supported by a Grant-in-Aid
442 for Scientific Research (C) (19K11716) to TU, (16K09168) to MM, (21K11671) to HI, a

443 Grant-in-Aid for Young Scientists (B) (15K19547) to TU from the Ministry of Education,
444 Culture, Sports, Science and Technology, Japan and the Japanese society of hematology
445 research grant (2017-2020) to TU. WSA was supported by grants from the Australian
446 National Health and Medical Research Council (1058344, 1173342, 1113577).

447

448 **AUTHOR CONTRIBUTIONS**

449 KC and TU designed all studies and wrote the manuscript. KC, TU, and HI performed
450 most of the experiments. ST, TS, TK, and MM performed FACS analyses. HI and MA
451 performed hepatic lipid analyses. KC, HI, RO, and YA performed pathological analyses.
452 IS analyzed physiological analyses data. TU and HH provided advice regarding
453 granulopoiesis. TU and SN analyzed bioinformatic data. TU, MW, YF, YN, HH, and WA
454 reviewed and edited the paper. TU, YN, WA, HS, and HS provided information regarding
455 all experiments.

456

457 **DECLARATION OF INTERESTS**

458 The authors declare no competing interests.

459

460

461 **Figure Legends**

462 **Fig 1. Effects of diet and genotype on body weight, liver fat, and glucose tolerance.**

463 (A) Weekly body weight gain. Mean ± SD is shown with ****p<0.0001 and **p<0.01

464 for the comparison of WT with HFD and S3 with HFD, or WT with chow and SOCS3KO

465 with chow at 28 weeks after birth, using the one-way ANOVA with Tukey's multiple

466 comparisons test, n = 3–22/group. (B, C) Total daily food intake, total daily caloric intake,

467 and lipid intake at 15 weeks of age, n = 6–9/group. Mean ± SD is shown with

468 ****p<0.0001, ***p<0.001, **p<0.01, and *p<0.05. (D) Liver pathology (hematoxylin

469 and eosin staining). (E) Hepatic total cholesterol and triglyceride levels on day 30 after

470 tamoxifen treatment, n = 5/group. Mean ± SD is shown with **p<0.01, and *p<0.05. Bar

471 = 100 μm. (F, G) Total distances and total movement duration in open field tests at 30

472 days after tamoxifen administration, n = 4–6/group. (H) Number of rotations with running

473 wheel system at 30 days after tamoxifen administration, n = 3–7/group. (I) Respiratory

474 exchange ratio at 30 days after tamoxifen administration, n = 3–5/group. Mean ± SD is

475 shown with ****p<0.0001, **p<0.01, and *p<0.05 (J) Casual blood glucose on day 14

476 after tamoxifen administration (left, n = 5–6/group). Mean ± SD is shown with *p<0.05

for comparison. (K) Insulin tolerance test on day 14 after tamoxifen administration (right, n = 5–6/group). # $p<0.05$ (WT-HFD vs. S3-chow), Ψ $p<0.05$ (WT-HFD vs. WT-chow) and $p<0.01$ (WT-HFD vs. S3-chow), θ$p<0.05$ (WT-HFD vs. WT-chow and S3-chow). (L) Serum leptin level at 30 days after tamoxifen administration. n = 9–12/group. Mean ± SD is shown with ***$p<0.001$. ND: normal diet, HFD: high fat diet, S3-HFD: SOCS3-deficient with HFD, S3-chow: SOCS3-deficient with chow, WT-HFD: $SOCS3^{fl/fl}$ with HFD, WT-chow: $SOCS3^{fl/fl}$ with chow.

Fig 2. SOCS3KO exacerbates rapid granulopoiesis with HFD in the blood and spleen. (A) Disease onset in mice with systemic SOCS3KO. ****$p<0.0001$, ***$p<0.001$, and **$p<0.01$ for the pairwise comparison of survival of S3-HFD (○) and S3-chow (●) or other control genotypes. Mantel-Cox Log-rank test, n = 15–28/group. (B) Peripheral blood counts and (C) spleen weight on day 30 following tamoxifen or vehicle administration, n = 6–15. (D) Spleen weight and (E) peripheral blood cell counts on day 65 following tamoxifen or vehicle administration, n = 4–13/group. (F) Images of representative live WT-HFD and S3-HFD mice on day 30 following tamoxifen or vehicle

493 administration. (G) Pathology in SOCS3-deficient mice on HFD. S3-HFD mice started
494 to show liver inflammation on day 30 after tamoxifen administration (left column), but
495 infiltration of inflammatory cells was not observed in fat, lung, and kidney. Moribund
496 S3-HFD mice showed obvious infiltration of inflammatory cells (right column). Arrows
497 indicate infiltrating inflammatory cells. Mean ± SD is shown with *p<0.05, **p<0.01,
498 ***p<0.001, and ****p<0.0001 for comparison.
499

500 **Fig 3. Characteristics of granulocytes and their maturation in the spleen.**

501 (A) Spleen pathology (hematoxylin and eosin stain) from mice with HFD on day 30 after
502 tamoxifen treatment. Bar = 100 μm. n = 8–12/group. (B) Granulocytes ($CD11b^+Gr\text{-}1^+$
503 cells) in the spleen on day 30 following tamoxifen or vehicle treatment, n = 3–7/group.
504 (C) After flow cytometric analysis, granulocyte differentiation and maturation stages
505 were classified from gates #1 to #5. (D) Flow cytometric analysis of granulopoiesis from
506 immature to mature stages in the spleen on day 30 after tamoxifen treatment. n = 5–
507 8/group. (E) Total colony number in MethoCult™ M3534 containing SCF, IL-3, and IL-

6, n = 3/group. Mean ± SD is shown with *p<0.05, **p<0.01, ***p<0.001, and ****p<0.0001 for comparison.

Fig 4. Features of inflammation and infiltration markers of myeloid series cells in the liver. (A) Photomicrograph showing inflammation and mixed hematopoietic infiltration of the liver in S3-HFD mice on day 30 following tamoxifen administration. Bar = 100μm. (B) Biochemical examinations on day 30 following tamoxifen administration. n = 6–9/group. (C) Inflammation markers: *TNF-α* and *IL-6* mRNA levels; Myeloid infiltration markers: *CD11b*, *F4/80*, *Ly6G*, and *CD68* mRNA levels. n = 3–6/group. (D) Inflammasome markers: *IL-1β* and *Caspase-1* mRNA levels on day 30 following tamoxifen or vehicle administration. n = 3–4/group. (E) Inflammasome markers on day 65 following tamoxifen or vehicle administration. n = 4–5/group. Mean ± SD is shown with *p<0.05, **p<0.01, ***p<0.001, and ****p<0.0001 for comparison, using the one-way ANOVA with Tukey's multiple comparisons test.

Fig 5. Effects of HFD diet on hematopoietic SOCS3-deficient mice.

(A) Disease onset in mice with systemic SOCS3KO. ****p<0.0001 for pairwise comparison of survival of S3-HFD (○), LysM-HFD (●), and LysM-chow (◆). Mantel-Cox Log-rank test, n = 12–18 mice/group. (B) Weekly body weight gain. Mean ± SD is shown with ****p<0.0001 for comparison of LysM-chow and LysM-HFD, or WT with chow and WT with HFD at 28 weeks after birth, using the one-way ANOVA with Tukey's multiple comparisons test, n = 13–26/group. (C) Liver fat pathology (hematoxylin and eosin staining), (D) hepatic total cholesterol and triglyceride levels in LysM-SOCS3KO mice at 12 weeks of age, n = 5/group. (E) Number of neutrophils in the blood at 30 days after HFD or chow intake, n = 7–11 in each group. (F) Spleen weight, n = 5–9 in each group. (G) Liver fat pathology (hematoxylin and eosin staining), (H) hepatic total cholesterol and triglyceride levels in Vav-SOCS3KO mice at 12 weeks old, n = 5 in each group. Mean ± SD is shown with **p<0.01, and *p<0.05. Bar = 100μm. (I) Numbers of neutrophils in the blood at 30 days in mice with hematopoietic SOCS3KO after HFD or chow intake, n = 3–12/group. (J) Spleen weight, n = 3–12 in each group. (K) Percentage of each fraction by flow cytometric analysis of murine granulopoiesis in the spleen at 30 days after tamoxifen administration. Mean ± SD is shown with *p<0.05

and **p<0.01 for comparison. LysM: mature myeloid-specific SOCS3KO mice, Vav: hematopoietic specific KO mice.

Fig 6. Effects of orally administered antibiotics for intestinal tract microbiota depletion.

Cocktails containing four antibiotics (Abx) were administered from 4 weeks of age. (A) The results of the principal coordinate analysis and (B) relative mean abundance of the operative taxonomic units (OTUs) in the fecal matter at the order level. Proportions of the first (PCoA1) and second (PCoA2) components are shown (n = 3/group). Four Abx-treated (WT-chow, WT-HFD, S3-chow, and S3-HFD) and four dots overlap at one point. (C) Disease onset in mice with SOCS3KO on HFD with four Abx (S3-HFD + 4Abx). Mantel-Cox Log-rank test, n = 7–18 mice/group. (D) Number of neutrophils in the blood (n = 4-14), (E) spleen weight (n = 4-12) and (F) number of granulocytes ($CD11b^{+}Gr\text{-}1^{+}$ cells) in the spleen (n = 3–7) on day 30, following tamoxifen or vehicle treatment with or without 4Abx. (G) Percentage of each murine granulopoiesis fraction, by flow cytometric analysis, in the spleen at 30 days after tamoxifen administration with or without 4Abx. n

= 4–8/group. Mean ± SD is shown with $^{\star}p<0.05$, $^{\star\star}p<0.01$, $^{\star\star\star}p<0.001$, and $^{\star\star\star\star}p<0.0001$ for comparison of S3-HFD with all phenotypes. (H) gut inflammation: *TNF-α* mRNA concentration in the colon on day 30 following tamoxifen administration with or without 4Abx. n = 3–4/group. Mean ± SD is shown with $^{**}p<0.05$, $^{**}p<0.01$, $^{***}p<0.001$, and $^{****}p<0.0001$ for comparison, One-way ANOVA with Tukey's multiple comparisons test. Four Abx; ampicillin, neomycin, metronidazole, and vancomycin.

Fig 7. Effects of intestinal tract microbiota depletion on myeloid hematopoiesis.

(A) Concentrations of cytokines/chemokines in the serum on day 30 following tamoxifen administration with or without 4Abx. n = 6–12/group. (B) Absolute numbers of BM cells, Lineage^{-}Sca-1^{+}c-Kit^{+} (LSK) cells, CD34^{-}LSK cells, CMP cells (Lineage^{-}Sca-1^{-}c-Kit^{+}CD16/32^{Low}CD34^{+}), GMP cells (Lineage^{-}Sca-1^{-}c-Kit^{+}CD16/32^{High}CD34^{+}), MEP cells (Lineage^{-}Sca-1^{-}c-Kit^{+}CD16/32^{-}CD34^{-}) in the femurs on day 30 following tamoxifen administration with or without 4Abx. n = 6–11/group. Mean ± SD is shown with $^{*}p<0.05$, $^{**}p<0.01$, and $^{***}p<0.001$ for comparison using the one-way ANOVA

572 with Tukey's multiple comparisons test.

573

574

STAR★METHODS

Detailed methods are provided in the online version of this paper and include the following:

- KEY RESOURCES TABLE
- RESOURCE AVAILABILITY
  - Lead Contact
  - Materials Availability
  - Data and Code Availability
- EXPERIMENTAL MODEL AND SUBJECT DETAILS
  - Animals and ethics statement
- METHOD DETAILS
  - Tamoxifen treatment and genotyping
  - High fat diet
  - Antibiotics treatment
  - Blood glucose measurement
  - Hepatic lipid analysis

- Hematology and flow cytometry
- Colony assay
- RT-PCR analysis
- Cytokine Luminex assay
- Physiological analyses
- Bacterial 16S rRNA amplicon sequencing and analysis

- **QUANTIFICATION AND STATISTICAL ANALYSIS**

STAR★METHODS

KEY RESOURCES TABLE

RESOURCE AVAILABILITY

Lead Contact

Further information and requests for resources and reagents should be directed to and will be fulfilled by the lead contact, Takashi Ushiki (tushiki@med.niigata-u.ac.jp).

Materials Availability

This study did not generate new unique reagents.

Data and Code Availability

- 16S rRNA amplicon sequencing was performed at Techno Suruga Laboratory, Inc. (Shizuoka, Japan). Bacterial identification from sequences was performed using the TechnoSuruga Lab Microbial Identification database DB-BA 13.0 (TechnoSuruga Laboratory).
- Microbiome sequencing data have been deposited at the DDBJ Sequence Read Archive (http://trace.ddbj.nig.ac.jp/dra/) under accession number DRA012691.

- All original code is available in this paper's supplemental information.
- Any additional information requires to reanalyze the data reported in this paper is available from the lead contact upon request.

EXPERIMENTAL MODEL AND SUBJECT DETAILS

Animals and ethics statement

SOCS3 floxed (*Socs3*^{fl}), Rosa26-CreERT2, LysM-Cre, and Vav-Cre mice have been described previously (Clausen et al., 1999; Joseph et al., 2013; Kiu et al., 2007; Seibler et al., 2003); they were maintained in a C57BL/6 background. In experimental mice, the Rosa26-CreERT2 and Vav-Cre alleles were heterozygous and LysM-Cre was homozygous. 4 weeks old male and female mice were randomly assigned to experiments for 8-24 weeks. All animal experiments in this study were performed with the approval of the Animal Ethics Committees of Niigata University (SA00520, SD01054) or Walter and Eliza Hall Institute of Medical Research Animal Ethics Committee (2011.031, 2014.029).

METHOD DETAILS

Tamoxifen treatment and genotyping

Tamoxifen (4.2 mg for two doses after 4 days) was administered by oral gavage at 8 weeks of age, as previously described (Anastassiadis et al., 2010). PCR genotyping was performed using the following primers to distinguish the *Socs3*$^{+}$ (613bp), *Socs3*^{fl} (740bp), and *Socs3*$^{-}$ (288bp) alleles: 5′-ACGTCTGTGATGCTTTGCTG-3′, 5′-TCTTGTGTCTCTCCCCATCC-3′, and 5′-TGACGCTCAACGTGAAGAAG-3′.

High fat diet

Mice of all genotypes were fed an HFD (D12492; 60 kcal % fat, Research Diet Inc., New Brunswick, NJ, USA) or control chow (D12450J; 10 kcal % fat, Research diet, Inc.) from 4 weeks of age to the end of the observation period.

Antibiotics treatment

For intestinal tract microbiota depletion, mice were administered the following cocktail of four antibiotics (4Abx) in their drinking water from 4 weeks of age: ampicillin (Sigma-Aldrich, Merck KGaA, Darmstadt, Germany) 1 g/L, neomycin (Sigma-Aldrich) 1 g/L,

647 metronidazole (Sigma-Aldrich) 1 g/L, and vancomycin (Nacalai Tesque, Inc., Kyoto,
648 Japan) 500 mg/L. The 4Abx treatment was continued during the observation period.

649 **Blood glucose measurement**

650 Serum blood glucose was measured using blood collected from the retro-orbital plexus
651 into Microtainer® tubes (BD Biosciences, Bedford, MA, USA) using Bio Majesty 6500
652 (JEOL Ltd., Tokyo, Japan). For the insulin tolerance test, 10-week-old mice were
653 administered intraperitoneal insulin injections (0.375 U/kg body weight) following 5.5 h
654 of fasting, blood was collected from the tail, and the glucose level was measured using a
655 blood glucose meter.

656 **Hepatic lipid analysis**

657 Total lipids were extracted from the liver as previously described (Kuba et al., 2015).
658 Hepatic T-Chol and TG were measured using the Cholesterol E-test and Triglyceride E-
659 test (Fujifilm Wako Pure Chemical, Osaka, Japan).

660 **Hematology and flow cytometry**

661 Cells in blood collected from the retro-orbital plexus into Microtainer® tubes containing
662 EDTA (BD biosciences, Bedford, MA, USA) were counted using Sysmex pocH-

100iVDiff (Sysmex corporation, Kobe, Japan). Flow cytometric analysis was performed using CytoFLEX (Beckman coulter, NJ, USA). Antibodies were sourced from Biolegend (CA, USA): CD3 (17A2), CD4 (GK1.5), CD8 (53–6.7), Gr-1 (RB6-8C5), CD11b (M1/70), CD34 (RAM34), c-Kit (ACK2), Ly6G (1A8), CD19 (6D5), B220 (RA3-6B2), and TER119 (TER-119). LSK, CMP, GMP and megakaryocyte-erythroid progenitor (MEP) cells were counted as previously described (Katagiri et al., 2021). Granulocyte maturation was assessed based on the expression of c-kit and Ly6G as previously described (Fig S6) (Satake et al., 2012).

Colony assay

BM cells (2.0×10^4) were harvested from 8–10-week old mice and cultured in MethoCult M3534 (Stem Cell Technologies, Vancouver, Canada) according to the manufacturer's instructions. Total number of colonies, colony forming unit-granulocyte/macrophage (CFU-GM, CFU-G, and CFU-M), was scored after 7 days of culture.

RT-PCR analysis

The total RNA was isolated from the liver and colon using the RNeasy Mini kit (Qiagen, Hilden, Germany) according to the manufacturer's instructions. Regarding liver samples,

679 RNA was collected without systemic perfusion. Reverse transcription of RNA to cDNA
680 was performed using the SuperScript Reverse Transcriptase III kit (Thermo Fisher
681 Scientific, MA, USA) with random hexamer primers. Each cDNA sample was analyzed
682 using quantitative PCR with the StepOnePlus™ Real-Time PCR System (Thermo
683 Fisher Scientific). Gene mRNA levels were determined by RT-qPCR using TaqMan
684 probes (Thermo Fisher Scientific) (Table S3). Samples were run in triplicate and relative
685 fold-changes in mRNA levels were calculated using the $2^{-\Delta\Delta Ct}$ method.

686 **Cytokine Luminex assay**

687 The serum concentrations of 20 cytokines (GM-CSF, CXCL1, TNFα, CCL2, IL-1β,
688 S100A8, S100A9, IL-6, IL-10, IL-13, IL-17A, IFNγ, IL-3, Leptin, CCL5, G-CSF, IL-33,
689 M-CSF, CCL3, and CCL4) were determined using the Luminex100/200 System
690 (Luminex Corporation, TX, USA). Data were analyzed using MILLIPLEX Analyst 5.1
691 (EMD Millipore Corporation, MA, USA).

692 **Physiological analyses**

693 Mice were individually housed to monitor body weight and food intake. Oxygen
694 consumption was measured at 30 days after tamoxifen administration using an O_2/CO_2

695 metabolic measurement system (Columbus Instruments, OH, USA), according to the
696 manufacturer's instruction. Spontaneous activity levels were measured at 30 days after
697 tamoxifen administration using the running wheel system and an open field test. Using
698 the Igloo Fast-Tracs Running Wheel system MK-713 (Muromachi Kikai, Tokyo, Japan),
699 mice were housed individually in a cage containing this system, and the data were
700 collected over 24 h using CompACT AMS Data Collection Software version 3.84
701 (Muromachi Kikai) following the training period for 12–16 h. In the open field test, each
702 mouse was placed in the corner of an enclosed platform (40 cm × 40 cm × 30 cm), and
703 the total distance traveled, time traveled, and time spent in the central area (20 cm × 20
704 cm) was recorded for 10 min.

705 **Bacterial 16S rRNA amplicon sequencing and analysis**

706 Fecal samples of mice at 30 days post-tamoxifen treatment were collected. 16S rRNA
707 amplicon sequencing was performed at Techno Suruga Laboratory, Inc. (Shizuoka,
708 Japan). In brief, bacterial genomic DNA was isolated as previously described (Takahashi
709 et al., 2014). The V3-V4 hypervariable regions of the 16S rRNA were amplified from
710 microbial genomic DNA using PCR with the bacterial universal primers (*341F/R806*)

711 (Caporaso et al., 2011; Muyzer et al., 1993) and the dual-index method. All amplicons
712 were sequenced on a MiSeq (Illumina, USA). The obtained read sequences on both sides
713 were joined using fastq_join. After extracting a sequence with a QV of more than 20 with
714 99% or more bases in the sequence, the chimeric sequence was removed using
715 USEARCH. Bacterial identification from sequences was performed using the
716 TechnoSuruga Lab Microbial Identification database DB-BA 13.0 (TechnoSuruga
717 Laboratory) and the results of RDP MultiClassifier ver.2.11 using Metagenome@KIN
718 analysis software (World Fusion, Japan). Comparative analyses were also performed
719 using Metagenome@KIN analysis software. In addition, we performed principal
720 coordinate analysis (PCoA). The Euclidean distance was calculated using genus relative
721 abundance in each sample. The PCoA was performed using the pcoa function in the R
722 "ape" library (Paradis and Schliep, 2019).
723

724 **QUANTIFICATION AND STATISTICAL ANALYSIS**

725 Unless otherwise stated, data were analyzed using the analysis of variance (ANOVA)
726 corrected for multiple testing. *P*-values for specific comparisons were determined using

GraphPad Prism (GraphPad Software, CA, USA). Further analyses are indicated in the figure legends. $P<0.05$ was considered significant.

731 **REFERENCES**

732 Anastassiadis, K., Glaser, S., Kranz, A., Berhardt, K., and Stewart, A.F.
733 (2010). A practical summary of site-specific recombination, conditional
734 mutagenesis, and tamoxifen induction of CreERT2. Methods Enzymol *477*,
735 109-123.

736 Atarashi, K., Tanoue, T., Shima, T., Imaoka, A., Kuwahara, T., Momose, Y.,
737 Cheng, G., Yamasaki, S., Saito, T., Ohba, Y., et al. (2011). Induction of colonic
738 regulatory T cells by indigenous Clostridium species. Science *331*, 337-341.

739 Cani, P.D., Amar, J., Iglesias, M.A., Poggi, M., Knauf, C., Bastelica, D.,
740 Neyrinck, A.M., Fava, F., Tuohy, K.M., Chabo, C., et al. (2007a). Metabolic
741 endotoxemia initiates obesity and insulin resistance. Diabetes *56*, 1761-1772.

742 Cani, P.D., Neyrinck, A.M., Fava, F., Knauf, C., Burcelin, R.G., Tuohy, K.M.,
743 Gibson, G.R., and Delzenne, N.M. (2007b). Selective increases of
744 bifidobacteria in gut microflora improve high-fat-diet-induced diabetes in
745 mice through a mechanism associated with endotoxaemia. Diabetologia *50*,
746 2374-2383.

747 Caporaso, J.G., Lauber, C.L., Walters, W.A., Berg-Lyons, D., Lozupone, C.A.,
748 Turnbaugh, P.J., Fierer, N., and Knight, R. (2011). Global patterns of 16S
749 rRNA diversity at a depth of millions of sequences per sample. Proc Natl Acad
750 Sci U S A *108 Suppl 1*, 4516-4522.

751 Chen, Z., Laurence, A., Kanno, Y., Pacher-Zavisin, M., Zhu, B.M., Tato, C.,
752 Yoshimura, A., Hennighausen, L., and O'Shea, J.J. (2006). Selective
753 regulatory function of Socs3 in the formation of IL-17-secreting T cells. Proc
754 Natl Acad Sci U S A *103*, 8137-8142.

755 Clausen, B.E., Burkhardt, C., Reith, W., Renkawitz, R., and Forster, I. (1999).
756 Conditional gene targeting in macrophages and granulocytes using LysMcre
757 mice. Transgenic Res *8*, 265-277.

758 Cornish, A.L., Davey, G.M., Metcalf, D., Purton, J.F., Corbin, J.E.,
759 Greenhalgh, C.J., Darwiche, R., Wu, L., Nicola, N.A., Godfrey, D.I., et al.
760 (2003). Suppressor of cytokine signaling-1 has IFN-gamma-independent
761 actions in T cell homeostasis. Journal of immunology (Baltimore, Md. : 1950)
762 *170*, 878-886.

763 Croker, B.A., Kiu, H., Pellegrini, M., Toe, J., Preston, S., Metcalf, D.,
764 O'Donnell, J.A., Cengia, L.H., McArthur, K., Nicola, N.A., et al. (2012). IL-6
765 promotes acute and chronic inflammatory disease in the absence of SOCS3.
766 Immunol Cell Biol *90*, 124-129.

767 Croker, B.A., Krebs, D.L., Zhang, J.G., Wormald, S., Willson, T.A., Stanley,
768 E.G., Robb, L., Greenhalgh, C.J., Forster, I., Clausen, B.E., et al. (2003).
769 SOCS3 negatively regulates IL-6 signaling in vivo. Nat Immunol *4*, 540-545.

770 Croker, B.A., Metcalf, D., Robb, L., Wei, W., Mifsud, S., DiRago, L., Cluse, L.A.,
771 Sutherland, K.D., Hartley, L., Williams, E., et al. (2004). SOCS3 is a critical
772 physiological negative regulator of G-CSF signaling and emergency
773 granulopoiesis. Immunity *20*, 153-165.

774 Davey, G.M., Starr, R., Cornish, A.L., Burghardt, J.T., Alexander, W.S.,
775 Carbone, F.R., Surh, C.D., and Heath, W.R. (2005). SOCS-1 regulates IL-15-
776 driven homeostatic proliferation of antigen-naive CD8 T cells, limiting their
777 autoimmune potential. J Exp Med *202*, 1099-1108.

778 Duan, Y., Zeng, L., Zheng, C., Song, B., Li, F., Kong, X., and Xu, K. (2018).

779 Inflammatory Links Between High Fat Diets and Diseases. Front Immunol
780 *9*, 2649.
781 Esplugues, E., Huber, S., Gagliani, N., Hauser, A.E., Town, T., Wan, Y.Y.,
782 O'Connor, W., Jr., Rongvaux, A., Van Rooijen, N., Haberman, A.M., et al.
783 (2011). Control of TH17 cells occurs in the small intestine. Nature *475*, 514-
784 518.
785 Furusawa, Y., Obata, Y., Fukuda, S., Endo, T.A., Nakato, G., Takahashi, D.,
786 Nakanishi, Y., Uetake, C., Kato, K., Kato, T., et al. (2013). Commensal
787 microbe-derived butyrate induces the differentiation of colonic regulatory T
788 cells. Nature *504*, 446-450.
789 Gromovsky, A.D., Schugar, R.C., Brown, A.L., Helsley, R.N., Burrows, A.C.,
790 Ferguson, D., Zhang, R., Sansbury, B.E., Lee, R.G., Morton, R.E., et al. (2018).
791 Delta-5 Fatty Acid Desaturase FADS1 Impacts Metabolic Disease by
792 Balancing Proinflammatory and Proresolving Lipid Mediators. Arterioscler
793 Thromb Vasc Biol *38*, 218-231.
794 Hirakata, S., Aoki, H., Ohno-Urabe, S., Nishihara, M., Furusho, A., Nishida,

795 N., Ito, S., Hayashi, M., Yasukawa, H., Imaizumi, T., et al. (2020). Genetic
796 Deletion of Socs3 in Smooth Muscle Cells Ameliorates Aortic Dissection in
797 Mice. JACC Basic Transl Sci *5*, 126-144.

798 Howard, J.K., Cave, B.J., Oksanen, L.J., Tzameli, I., Bjorbaek, C., and Flier,
799 J.S. (2004). Enhanced leptin sensitivity and attenuation of diet-induced
800 obesity in mice with haploinsufficiency of Socs3. Nat Med *10*, 734-738.

801 Inagaki-Ohara, K., Mayuzumi, H., Kato, S., Minokoshi, Y., Otsubo, T.,
802 Kawamura, Y.I., Dohi, T., Matsuzaki, G., and Yoshimura, A. (2014).
803 Enhancement of leptin receptor signaling by SOCS3 deficiency induces
804 development of gastric tumors in mice. Oncogene *33*, 74-84.

805 Inoue, H., Ogawa, W., Asakawa, A., Okamoto, Y., Nishizawa, A., Matsumoto,
806 M., Teshigawara, K., Matsuki, Y., Watanabe, E., Hiramatsu, R., et al. (2006).
807 Role of hepatic STAT3 in brain-insulin action on hepatic glucose production.
808 Cell Metab *3*, 267-275.

809 Jorgensen, S.B., O'Neill, H.M., Sylow, L., Honeyman, J., Hewitt, K.A.,
810 Palanivel, R., Fullerton, M.D., Oberg, L., Balendran, A., Galic, S., et al. (2013).

811 Deletion of skeletal muscle SOCS3 prevents insulin resistance in obesity.
812 Diabetes *62*, 56-64.
813 Joseph, C., Quach, J.M., Walkley, C.R., Lane, S.W., Lo Celso, C., and Purton,
814 L.E. (2013). Deciphering hematopoietic stem cells in their niches: a critical
815 appraisal of genetic models, lineage tracing, and imaging strategies. Cell
816 Stem Cell *13*, 520-533.
817 Katagiri, T., Uemura, S., Ushiki, T., Nakajima-Takagi, Y., Oshima, M.,
818 Mikami, T., Kawasaki, A., Ishiguro, H., Tanaka, T., Sone, H., et al. (2021).
819 Distinct effects of chondroitin sulfate on hematopoietic cells and the stromal
820 microenvironment in bone marrow hematopoiesis. Exp Hematol *96*, 52-62.e55.
821 Kiu, H., Hilton, D.J., Nicola, N.A., Ernst, M., Marquez, R., Alexander, W.S.,
822 Roberts, A.W., and McManus, E.J. (2007). Mechanism of crosstalk inhibition
823 of IL-6 signaling in response to LPS and TNFalpha. Growth Factors *25*, 319-
824 328.
825 Kroy, D.C., Beraza, N., Tschaharganeh, D.F., Sander, L.E., Erschfeld, S.,
826 Giebeler, A., Liedtke, C., Wasmuth, H.E., Trautwein, C., and Streetz, K.L.

827 (2010). Lack of interleukin-6/glycoprotein 130/signal transducers and
828 activators of transcription-3 signaling in hepatocytes predisposes to liver
829 steatosis and injury in mice. Hepatology *51*, 463-473.
830 Kuba, M., Matsuzaka, T., Matsumori, R., Saito, R., Kaga, N., Taka, H.,
831 Ikehata, K., Okada, N., Kikuchi, T., Ohno, H., et al. (2015). Absence of Elovl6
832 attenuates steatohepatitis but promotes gallstone formation in a lithogenic
833 diet-fed Ldlr(-/-) mouse model. Sci Rep *5*, 17604.
834 Lesina, M., Kurkowski, M.U., Ludes, K., Rose-John, S., Treiber, M., Klöppel,
835 G., Yoshimura, A., Reindl, W., Sipos, B., Akira, S., et al. (2011). Stat3/Socs3
836 activation by IL-6 transsignaling promotes progression of pancreatic
837 intraepithelial neoplasia and development of pancreatic cancer. Cancer Cell
838 *19*, 456-469.
839 Liu, X., Miyazaki, M., Flowers, M.T., Sampath, H., Zhao, M., Chu, K., Paton,
840 C.M., Joo, D.S., and Ntambi, J.M. (2010). Loss of Stearoyl-CoA desaturase-1
841 attenuates adipocyte inflammation: effects of adipocyte-derived oleate.
842 Arterioscler Thromb Vasc Biol *30*, 31-38.

843 Luo, Y., Chen, G.L., Hannemann, N., Ipseiz, N., Kronke, G., Bauerle, T.,
844 Munos, L., Wirtz, S., Schett, G., and Bozec, A. (2015). Microbiota from Obese
845 Mice Regulate Hematopoietic Stem Cell Differentiation by Altering the Bone
846 Niche. Cell Metab *22*, 886-894.
847 Mori, H., Hanada, R., Hanada, T., Aki, D., Mashima, R., Nishinakamura, H.,
848 Torisu, T., Chien, K.R., Yasukawa, H., and Yoshimura, A. (2004). Socs3
849 deficiency in the brain elevates leptin sensitivity and confers resistance to
850 diet-induced obesity. Nat Med *10*, 739-743.
851 Muyzer, G., de Waal, E.C., and Uitterlinden, A.G. (1993). Profiling of complex
852 microbial populations by denaturing gradient gel electrophoresis analysis of
853 polymerase chain reaction-amplified genes coding for 16S rRNA. Appl
854 Environ Microbiol *59*, 695-700.
855 Ohno-Urabe, S., Aoki, H., Nishihara, M., Furusho, A., Hirakata, S., Nishida,
856 N., Ito, S., Hayashi, M., Yasukawa, H., Imaizumi, T., et al. (2018). Role of
857 Macrophage Socs3 in the Pathogenesis of Aortic Dissection. J Am Heart Assoc
858 *7*.

859 Oishi, Y., Spann, N.J., Link, V.M., Muse, E.D., Strid, T., Edillor, C., Kolar,
860 M.J., Matsuzaka, T., Hayakawa, S., Tao, J., et al. (2017). SREBP1 Contributes
861 to Resolution of Pro-inflammatory TLR4 Signaling by Reprogramming Fatty
862 Acid Metabolism. Cell Metab *25*, 412-427.
863 Paradis, E., and Schliep, K. (2019). ape 5.0: an environment for modern
864 phylogenetics and evolutionary analyses in R. Bioinformatics *35*, 526-528.
865 Qin, H., Wang, L., Feng, T., Elson, C.O., Niyongere, S.A., Lee, S.J., Reynolds,
866 S.L., Weaver, C.T., Roarty, K., Serra, R., et al. (2009). TGF-beta promotes
867 Th17 cell development through inhibition of SOCS3. J Immunol *183*, 97-105.
868 Roberts, A.W., Robb, L., Rakar, S., Hartley, L., Cluse, L., Nicola, N.A., Metcalf,
869 D., Hilton, D.J., and Alexander, W.S. (2001). Placental defects and embryonic
870 lethality in mice lacking suppressor of cytokine signaling 3. Proc Natl Acad
871 Sci U S A *98*, 9324-9329.
872 Sachithanandan, N., Fam, B.C., Fynch, S., Dzamko, N., Watt, M.J., Wormald,
873 S., Honeyman, J., Galic, S., Proietto, J., Andrikopoulos, S., et al. (2010). Liver-
874 specific suppressor of cytokine signaling-3 deletion in mice enhances hepatic

875 insulin sensitivity and lipogenesis resulting in fatty liver and obesity.
876 Hepatology *52*, 1632-1642.
877 Satake, S., Hirai, H., Hayashi, Y., Shime, N., Tamura, A., Yao, H., Yoshioka,
878 S., Miura, Y., Inaba, T., Fujita, N., et al. (2012). C/EBPbeta is involved in the
879 amplification of early granulocyte precursors during candidemia-induced
880 "emergency" granulopoiesis. J Immunol *189*, 4546-4555.
881 Seibler, J., Zevnik, B., Kuter-Luks, B., Andreas, S., Kern, H., Hennek, T.,
882 Rode, A., Heimann, C., Faust, N., Kauselmann, G., et al. (2003). Rapid
883 generation of inducible mouse mutants. Nucleic Acids Res *31*, e12.
884 Swiderski, K., Thakur, S.S., Naim, T., Trieu, J., Chee, A., Stapleton, D.I.,
885 Koopman, R., and Lynch, G.S. (2016). Muscle-specific deletion of SOCS3
886 increases the early inflammatory response but does not affect regeneration
887 after myotoxic injury. Skelet Muscle *6*, 36.
888 Tadokoro, Y., Hoshii, T., Yamazaki, S., Eto, K., Ema, H., Kobayashi, M., Ueno,
889 M., Ohta, K., Arai, Y., Hara, E., et al. (2018). Spred1 Safeguards
890 Hematopoietic Homeostasis against Diet-Induced Systemic Stress. Cell Stem

Cell *22*, 713-725.e718.

Takahashi, S., Tomita, J., Nishioka, K., Hisada, T., and Nishijima, M. (2014). Development of a prokaryotic universal primer for simultaneous analysis of Bacteria and Archaea using next-generation sequencing. PLoS One *9*, e105592.

Turnbaugh, P.J., Ley, R.E., Mahowald, M.A., Magrini, V., Mardis, E.R., and Gordon, J.I. (2006). An obesity-associated gut microbiome with increased capacity for energy harvest. Nature *444*, 1027-1031.

Ueki, K., Kondo, T., Tseng, Y.H., and Kahn, C.R. (2004). Central role of suppressors of cytokine signaling proteins in hepatic steatosis, insulin resistance, and the metabolic syndrome in the mouse. Proc Natl Acad Sci U S A *101*, 10422-10427.

Ushiki, T., Huntington, N.D., Glaser, S.P., Kiu, H., Georgiou, A., Zhang, J.G., Metcalf, D., Nicola, N.A., Roberts, A.W., and Alexander, W.S. (2016). Rapid Inflammation in Mice Lacking Both SOCS1 and SOCS3 in Hematopoietic Cells. PLoS One *11*, e0162111.

907

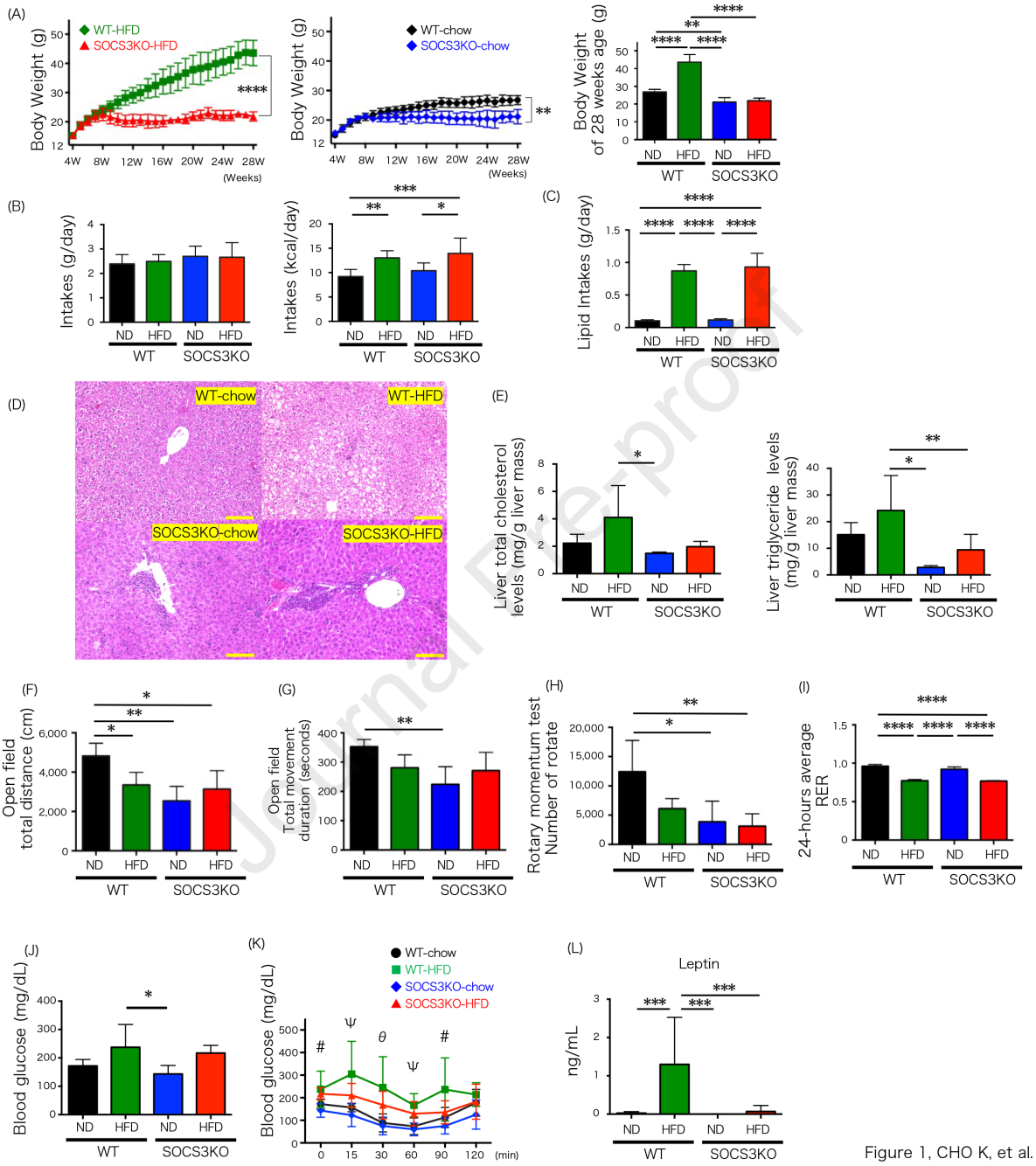

Figure 1, CHO K, et al.

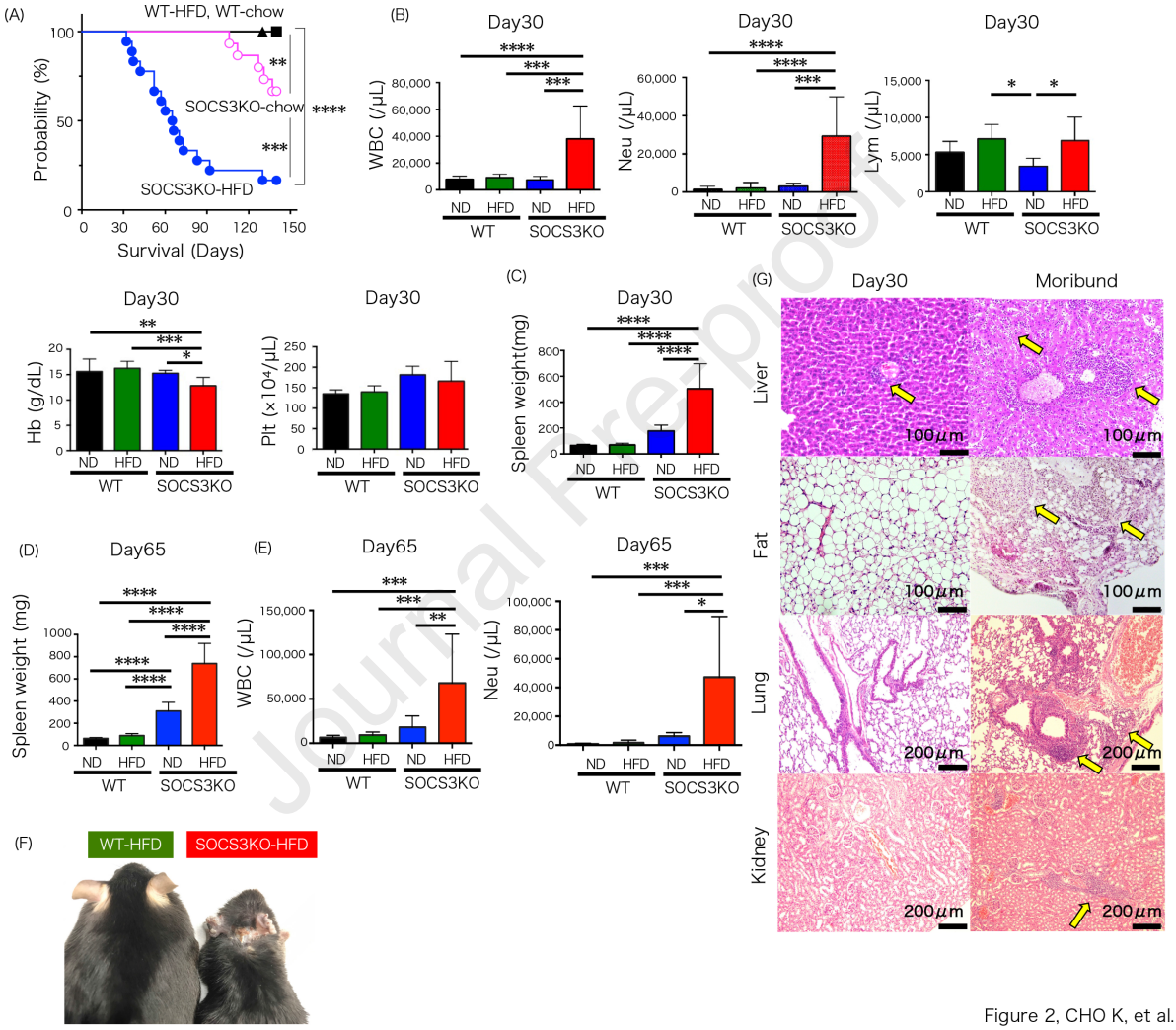

Figure 2, CHO K, et al.

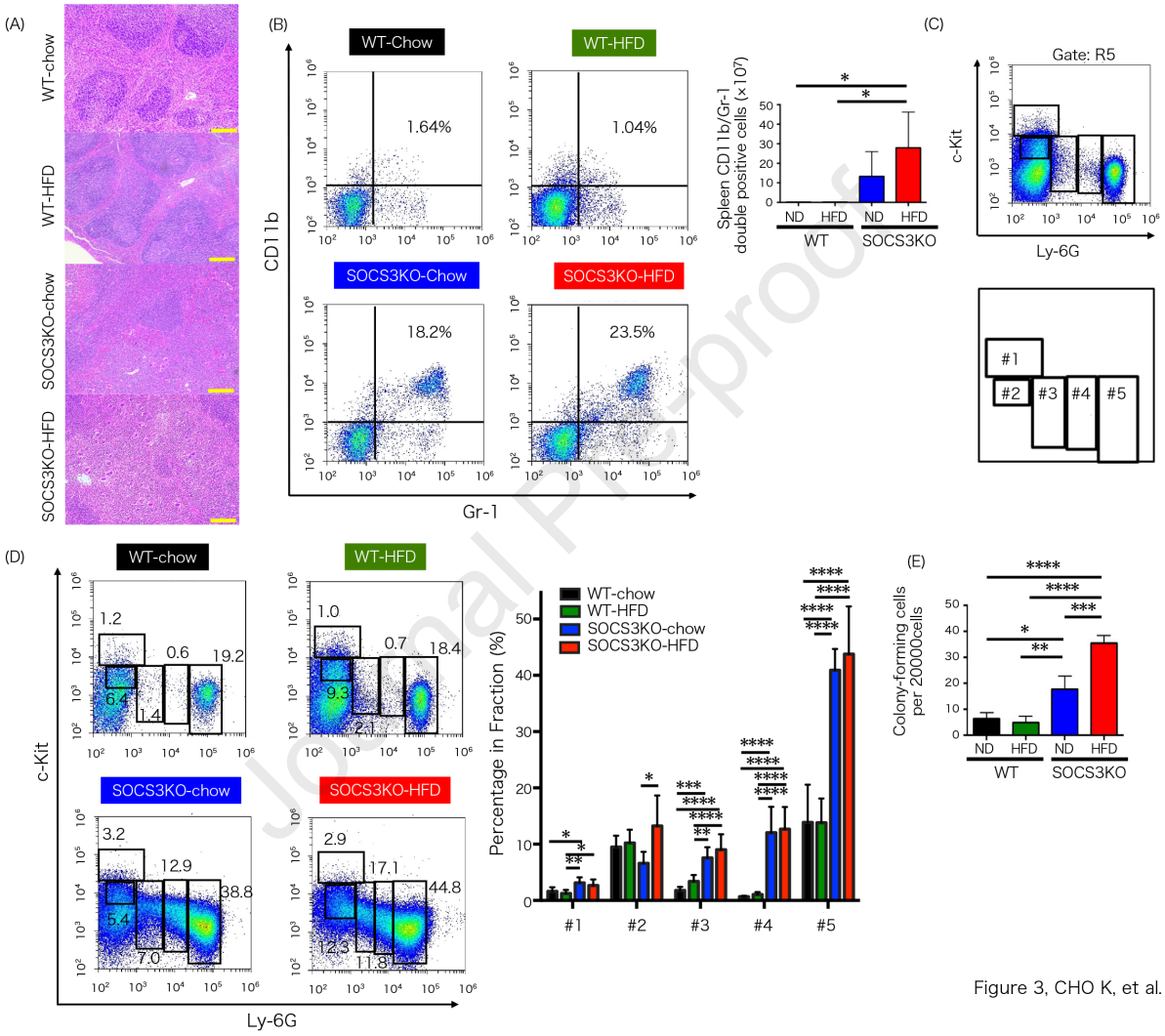

Figure 3, CHO K, et al.

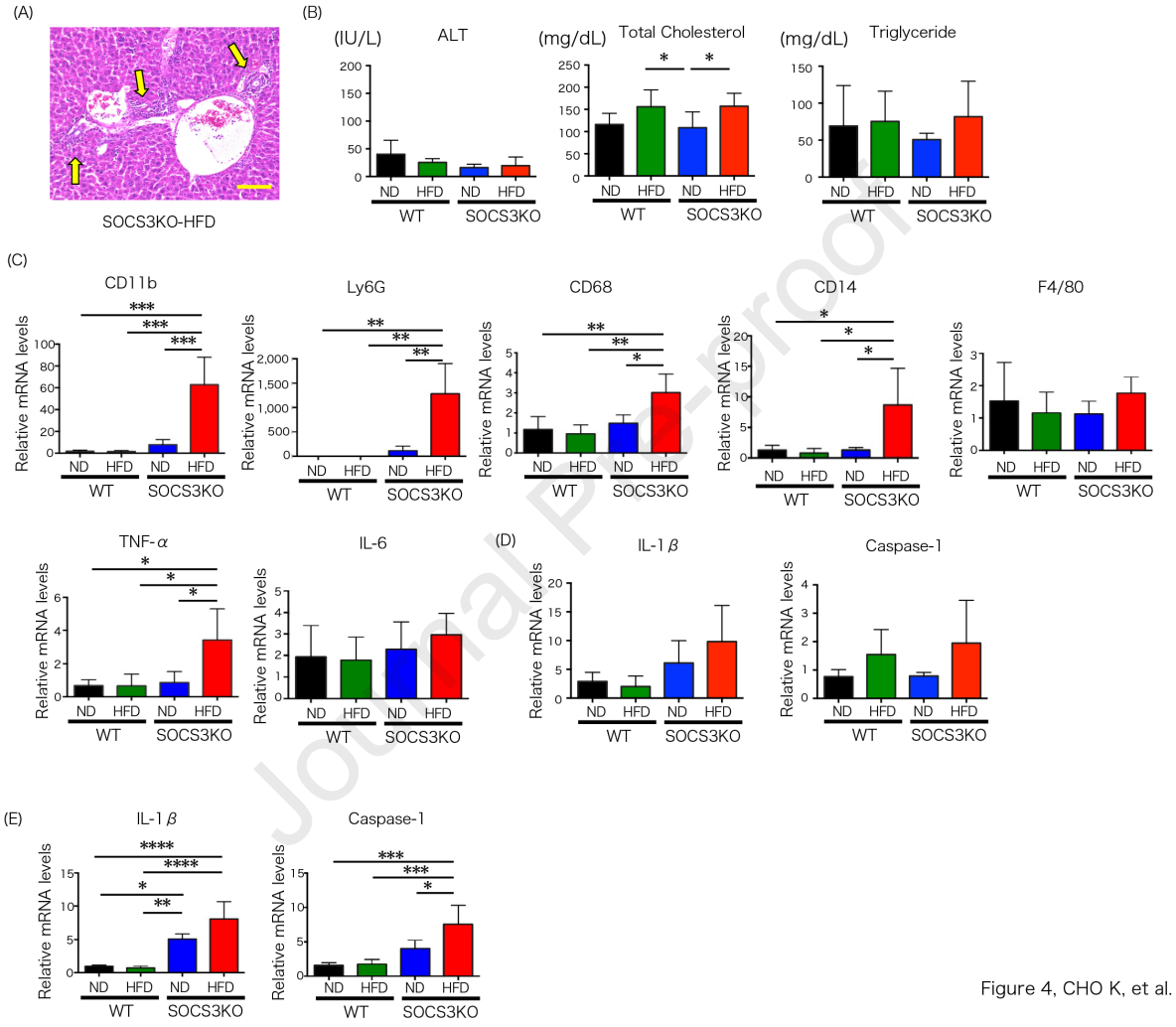

Figure 4, CHO K, et al.

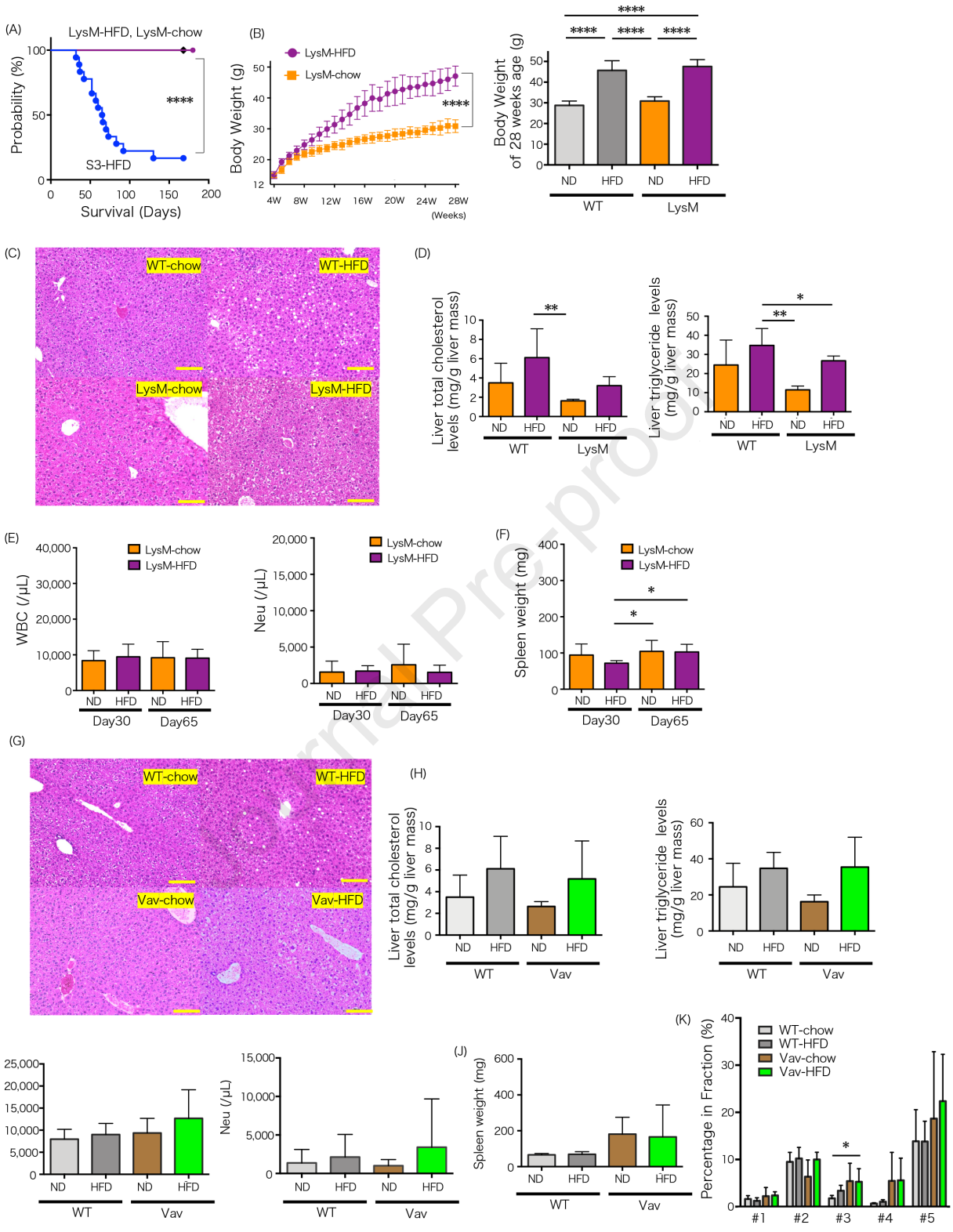

Figure 5, CHO K, et al.

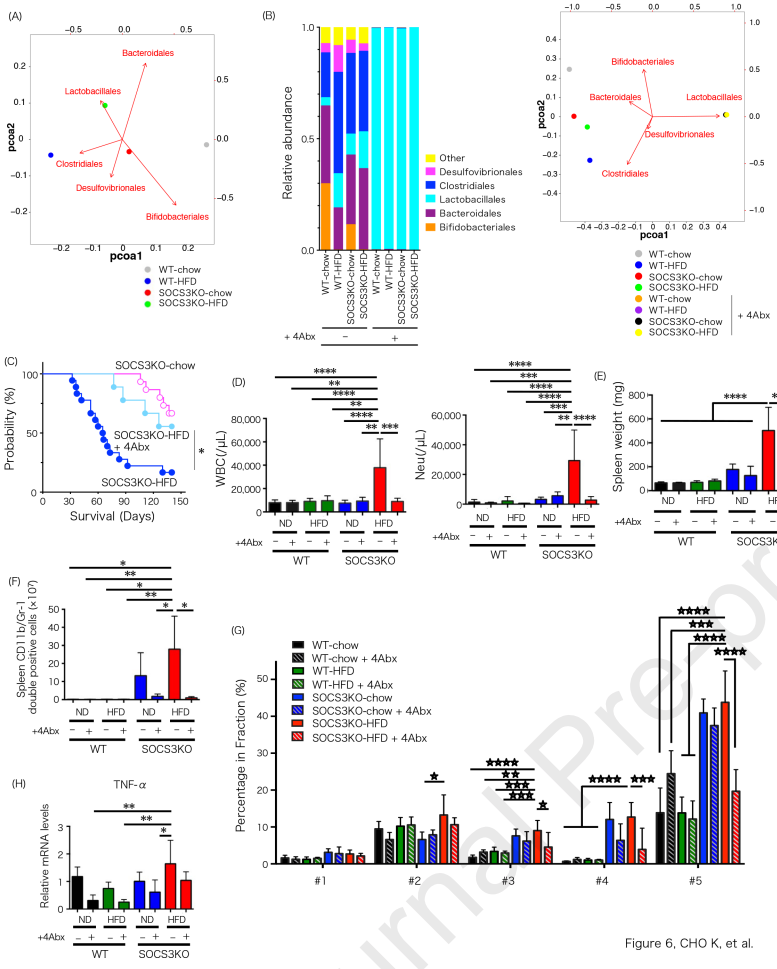

Figure 6, CHO K, et al.

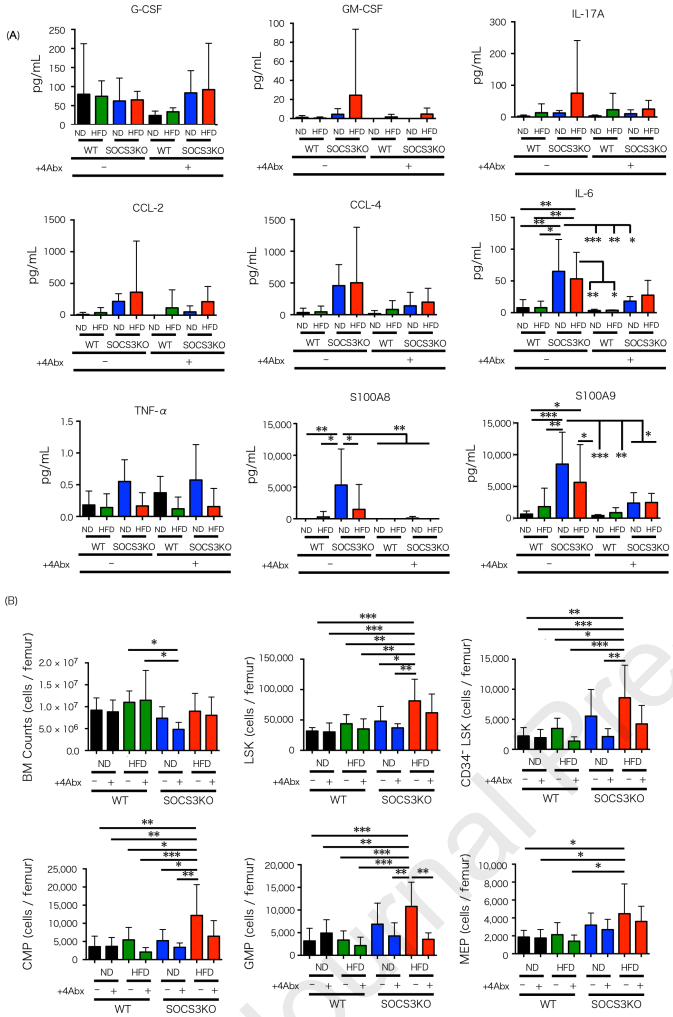

Figure 7, CHO K, et al.

Highlights

- SOCS3 suppresses severe systemic inflammation associated with high fat diet.
- SOCS3 deficiency on high fat diet accelerates excess myeloid hematopoiesis.
- SOCS3 controls gut dysbiosis on high fat diet.

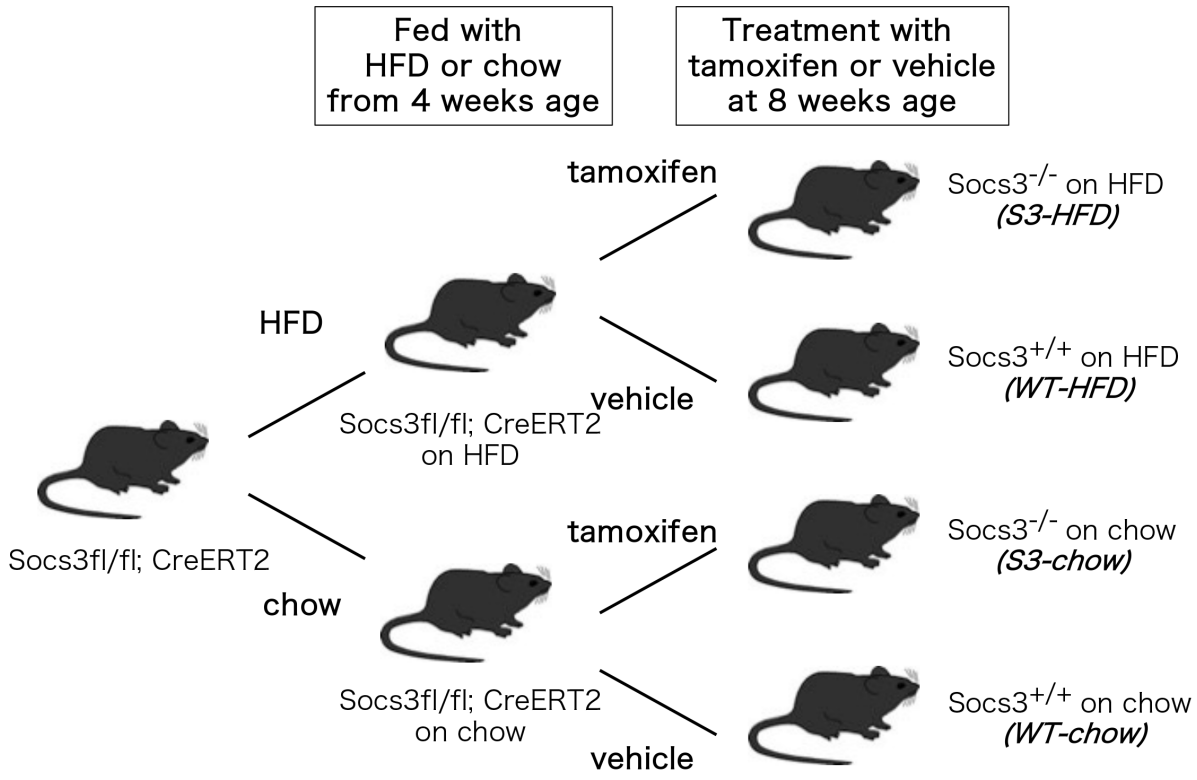

Figure S1. Experimental design for the generation of mice completely lacking SOCS3, Related to Figure 1.

High-fat diets were administered to the mice from 4 weeks of age. Tamoxifen and vehicle were administered at 8 weeks age for *in vivo* knockout of SOCS3.

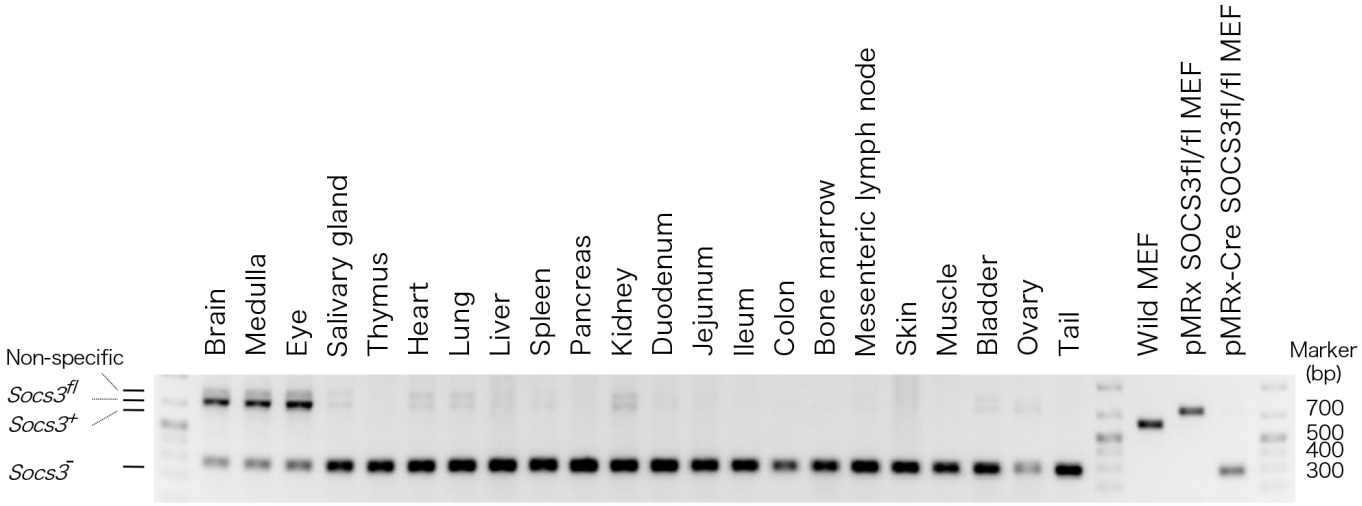

Figure S2. SOCS3KO rate in the organs after tamoxifen treatment, Related to Figure 1 and Figure 2.

To determine SOCS3KO efficiency in SOCS3$^{fl/fl}$Rosa26-CreERT2$^{KI/+}$ mice, tamoxifen (4.2 mg for two consecutive days) was administered by oral gavage at 8 weeks of age. PCR genotyping was performed using the following primers to distinguish the *Socs3*$^{+}$ (613bp), *Socs3*^{fl} (740bp), and *Socs3*$^{-}$ (288bp) alleles: 5′-ACGTCTGTGATGCTTTGCTG-3′, 5′-TCTTGTGTCTCTCCCCATCC-3′, and 5′-TGACGCTCAACGTGAAGAAG-3′. Intracranial organs, such as brain, medulla, and eye did not achieve complete SOCS3 KO due to the blood–brain barrier; however, other trunk organs achieved efficient SOCS3 KO on day 7 after tamoxifen treatment. Representative image is shown. WT (+), wild-type allele; fl, floxed allele; Δ, recombined, deleted allele; MEF, mouse embryonic fibroblast.

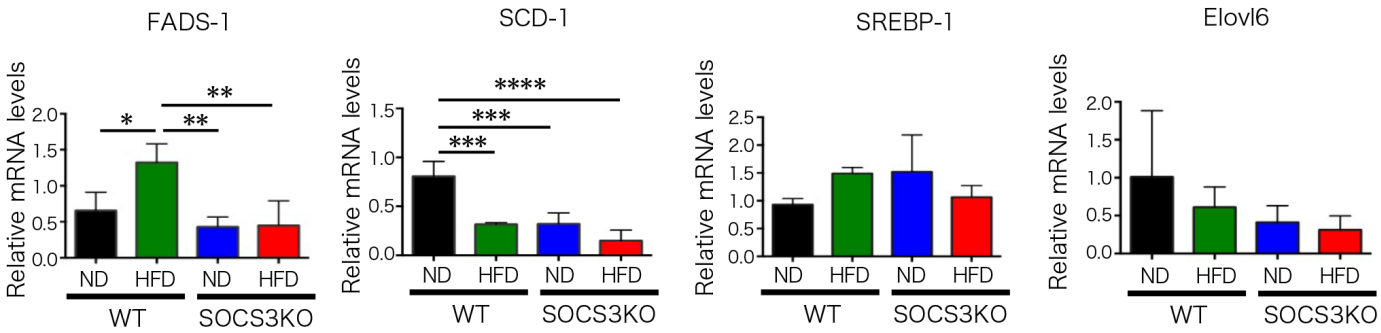

Figure S3. Features of fatty acid metabolism markers in the liver, Related to Figure 4.

Fatty acid metabolism markers: *FADS1*, *SCD1*, *SREBP-1*, and *Elovl6* on day 30 following tamoxifen or vehicle treatment. Mean ± SD is shown with **p*<0.05, ***p*<0.01, ****p*<0.001, and *****p*<0.0001 for comparison, using the one-way ANOVA with Tukey's multiple comparisons test, n = 3–6/group.

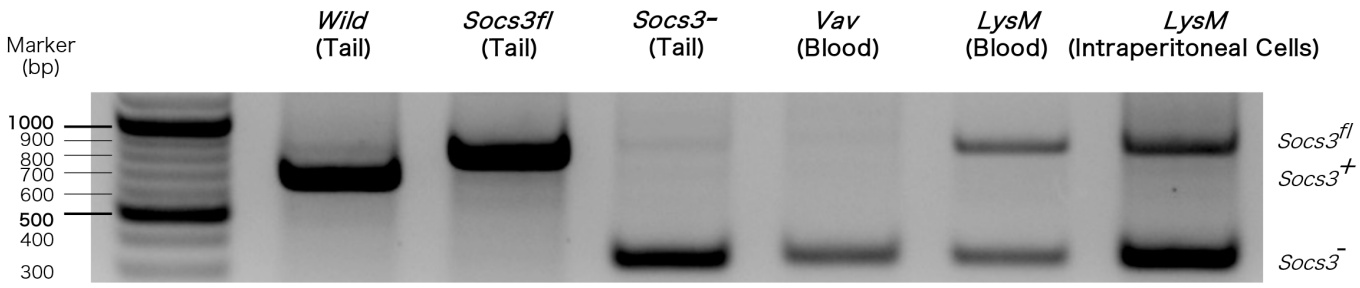

Figure S4. SOCS3KO rate in the organs after tamoxifen treatment, Related to Figure 5.

SOCS3KO efficiency in *VavCre Socs3*$^{fl/fl}$ (*Vav*) and *LysMCre Socs3*$^{fl/fl}$ (*LysM*) mice was analyzed at 12–15 weeks of age. Intraperitoneal cells include macrophages. PCR genotyping was performed using the following primers to distinguish the *Socs3*$^{+}$ (613bp), *Socs3*^{fl} (740bp), and *Socs3*$^{-}$ (288bp) alleles: 5′-ACGTCTGTGATGCTTTGCTG-3′, 5′-TCTTGTGTCTCTCCCCATCC-3′, and 5′-TGACGCTCAACGTGAAGAAG-3′. Representative image is shown. WT (+), wild-type allele; fl, floxed allele; Δ, recombined, deleted allele.

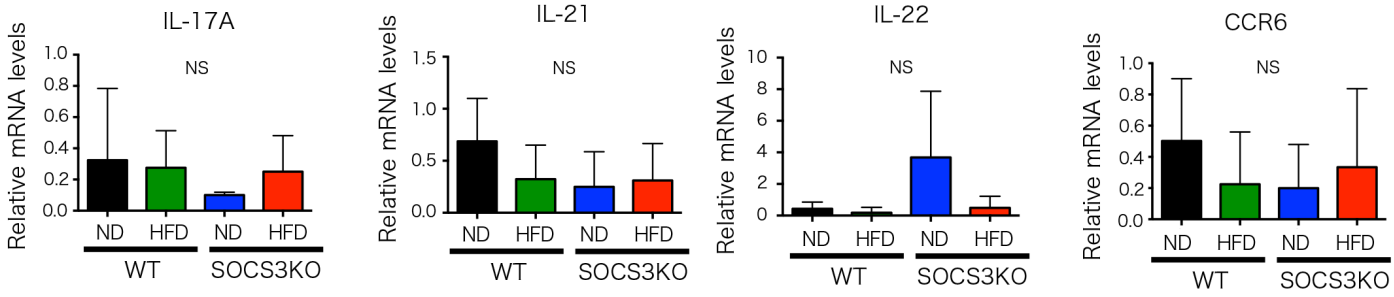

Figure S5. Features of Th-17 cell-related markers in the duodenum, Related to Figure 7A.

Th-17 cell-related markers *IL-17a*, *IL-21*, *IL-22*, and *CCR6* on day 30 following tamoxifen or vehicle treatment. Mean ± SD is shown; one-way ANOVA with Tukey's multiple comparisons test, n = 4/group. NS, not significant.

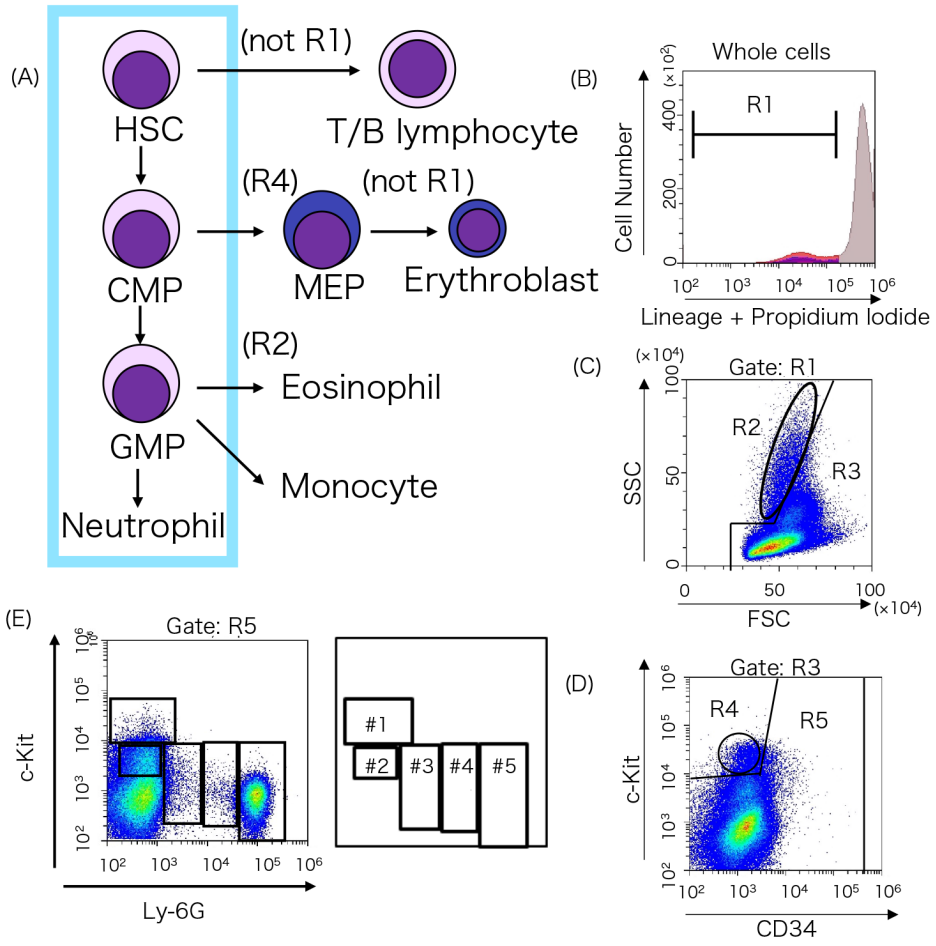

Figure S6. Flow cytometric analysis of murine granulopoiesis in the spleen, Related to Figure 3.

Murine granulopoiesis in the spleen was evaluated, as previously described (Satake S, *et al*., 2012). (A) Strategy used for flow cytometric analysis of mouse granulopoiesis. (B–E) Staining and gating of mouse spleen cells. First, the cells that had lost the potential to give rise to granulocytes were removed from the target population (B–D). The remaining cells (R5) were then analyzed for the expression of c-Kit and Ly-6G (E). Subpopulation #1 was c-Kit^{high}Ly-6G^{-}, #2 was c-Kit^{int}Ly-6G^{-}, and #5 was a discrete c-Kit^{low}Ly-6G^{high}. The remaining cells between #2 and #5 were divided into subpopulations #3 and #4 according to their expression levels of Ly-6G (E). After the flow cytometric identification, granulocyte differentiation and maturation stages were classified as indicated: Subpopulation #1 comprised mainly myeloblasts, #2 contained an abundance of promyelocytes, #3 mainly myelocytes, #4 mainly metamyelocytes, and #5 mainly band cells and segmented cells. HSC, hematopoietic stem cell; CMP, common myeloid progenitor; GMP, granulocyte-macrophage progenitor; MEP, megakaryocyte-erythroid progenitor; Ery, erythrocyte; 7-AAD, 7-amino-actinomycin D. n = 5–8/group. Mean ± SD is shown with *p<0.05, **p<0.01, ***p<0.001, and ****p<0.0001 for comparison.

Table S1. Pathological analyses on day 30 following tamoxifen administration with or without 4Abx, Related to Figure1A and Figure 7B.

					+4Abx			
	WT -chow	WT -HFD	SOCS3KO -chow	SOCS3KO -HFD	WT -chow	WT -HFD	SOCS3KO -chow	SOCS3KO -HFD
No. cases	2	2	3	3	3	3	3	3
Bone Marrow								
Myeloid hyperplasia	0	0	3	3	1	0	2	3
Slight erythroid hypoplasia	0	0	3	3	0	0	2	3
Megakaryocytosis	0	0	2	0	0	0	2	3
Pancreas								
Tumor	0	0	0	0	0	0	0	0
Stomach								
Tumor	0	0	0	0	0	0	0	0

Table S2. Gram staining of the organs on day 30 following tamoxifen administration with or without 4Abx, Related to Figure 7B.

					+4Abx			
	WT -chow	WT -HFD	SOCS3KO -chow	SOCS3KO -HFD	WT -chow	WT -HFD	SOCS3KO -chow	SOCS3KO -HFD
No. cases	2	2	3	3	3	3	3	3
Bone Marrow								
Bacteria	negative	negative	negative	negative	negative	negative	negative	negative

Table S3. TaqMan probes, Related to STAR Methods

Name	Source	Assay ID
CD11b	Thermo Fisher SCIENTIFIC	Mm00434455_m1
Ly6G	Thermo Fisher SCIENTIFIC	Mm04934123_m1
CD68	Thermo Fisher SCIENTIFIC	Mm03047343_m1
CD14	Thermo Fisher SCIENTIFIC	Mm00438094_g1
F4/80	Thermo Fisher SCIENTIFIC	Mm00802529_m1
TNF-α	Thermo Fisher SCIENTIFIC	Mm00443258_m1
IL-6	Thermo Fisher SCIENTIFIC	Mm00446190_m1
FADS-1	Thermo Fisher SCIENTIFIC	Mm00507605_m1
SCD-1	Thermo Fisher SCIENTIFIC	Mm00772290_m1
SREBP-1	Thermo Fisher SCIENTIFIC	Mm00550338_m1
Elovl6	Thermo Fisher SCIENTIFIC	Mm00851223_s1
IL-1β	Thermo Fisher SCIENTIFIC	Mm00434228_m1
IL-18	Thermo Fisher SCIENTIFIC	Mm00434226_m1
Caspase-1	Thermo Fisher SCIENTIFIC	Mm00438023_m1
IL-17A	Thermo Fisher SCIENTIFIC	Mm00439618_m1
IL-21	Thermo Fisher SCIENTIFIC	Mm00517640_m1
IL-22	Thermo Fisher SCIENTIFIC	Mm01226722_g1
CCR6	Thermo Fisher SCIENTIFIC	Mm99999114_s1
GAPDH	Thermo Fisher SCIENTIFIC	Mm99999915_g1